BRNO UNIVERSITY OF TECHNOLOGY
VYSOKÉ UČENÍ TECHNICKÉ V BRNĚ

FACULTY OF MECHANICAL ENGINEERING
FAKULTA STROJNÍHO INŽENÝRSTVÍ

INSTITUTE OF PHYSICAL ENGINEERING
ÚSTAV FYZIKÁLNÍHO INŽENÝRSTVÍ

DESIGN, FABRICATION AND TESTING OF GRAPHENE BIOSENSORS
NÁVRH, VÝROBA A TESTOVÁNÍ GRAFENOVÝCH BIOSENZORŮ

MASTER'S THESIS
DIPLOMOVÁ PRÁCE

AUTHOR — **Bc. Andrej Tripský**
AUTOR PRÁCE

SUPERVISOR — **doc. Ing. Miroslav Bartošík, Ph.D.**
VEDOUCÍ PRÁCE

BRNO 2020

BRNO UNIVERSITY OF TECHNOLOGY
FACULTY OF MECHANICAL ENGINEERING

Specification Master's Thesis

Department:	Institute of Physical Engineering
Student:	**Bc. Andrej Tripský**
Study programme:	Applied Sciences in Engineering
Study branch:	Physical Engineering and Nanotechnology
Supervisor:	**doc. Ing. Miroslav Bartošík, Ph.D.**
Academic year:	2019/20

Pursuant to Act no. 111/1998 concerning universities and the BUT study and examination rules, you have been assigned the following topic by the institute director Master's Thesis:

Design, fabrication and testing of graphene biosensors

Concise characteristic of the task:

Graphene due to its biocompatibility and high electronic mobility on a presence of adsorbed molecules is a suitable material for future electronic biosensors. The main topic of this diploma thesis will be to fabricate and test two types of graphene biosensors based on field effect transistor (FET) with a top electrolytical gate electrode. The first type of biosensor will be supported by a polymer substrate which is especially useful for medicine applications, the second type of biosensor will be supported by silicon and silicone dioxide substrate, which is more used in electronic applications. The second type of sensor will also be equipped by a bottom electronic gate. The goal of the work will be to compare the transport response both of these sensor types on a presence of a suitable chemical species, and evaluate the efficiency of a bottom gate in case of a second type of sensor.

Goals Master's Thesis:

1. Perform literature retrieval related to the design and fabrication of graphene biosensors.
2. Design and fabricate a biosensor on a polymer substrate with a top electrolytical gate electrode.
3. Design and fabricate a biosensor on a Si/SiO2 substrate with a top electrolytical gate electrode and a bottom electronic gate electrode.

Recommended bibliography:

ANG, Priscilla Kailian, Wei CHEN, Andrew Thye Shen WEE a Kian Ping LOH. Solution-Gated Epitaxial Graphene as pH Sensor. Journal of the American Chemical Society. 2008, 130(44), 14392–14393. DOI: 10.1021/ja805090z.

MACEDO, Lucyano J. A., Rodrigo M. IOST, Ayaz HASSAN, Kannan BALASUBRAMANIAN a Frank N. CRESPILHO. Bioelectronics and Interfaces Using Monolayer Graphene. ChemElectroChem. 2019, 6, 31–59. DOI: 10.1002/celc.201800934.

HELLER, Iddo, Sohail CHATOOR, Jaan MÄNNIK, Marcel A. G. ZEVENBERGEN, Cees DEKKER a Serge G. LEMEY. Influence of Electrolyte Composition on Liquid-Gated Carbon Nanotube and Graphene Transistors. Journal of the American Chemical Society. 2010, 132(48), 17149–17156. DOI: 10.1021/ja104850n.

OHNO, Yasuhide, Kenzo MAEHASHI, Yusuke YAMASHIRO a Kazuhiko MATSUMOTO. Electrolyte-Gated Graphene Field-Effect Transistors for Detecting pH and Protein Adsorption. Nano Letters. 2009, 9(9), 3318-3322. DOI: 10.1021/nl901596m.

Deadline for submission Master's Thesis is given by the Schedule of the Academic year 2019/20

In Brno,

L. S.

prof. RNDr. Tomáš Šikola, CSc. Director of the Institute	doc. Ing. Jaroslav Katolický, Ph.D. FME dean

ABSTRACT

The progress in nanotechnology gives an outstanding tool to develop new cutting edge devices. This thesis aims to fabricate, describe and measure graphene pH sensors on two different substrates - polymer parylene C and SiO_2. Such pH sensor is a pioneering step in the development of a wearable patch monitoring skin wound condition and local infections. Graphene is a one atom thick carbon-based material with promising properties and applications. We successfully performed two different experiments to characterise graphene sensors and their response to various pH. The first type of experiment used a liquid top gate to determine graphene charge neutrality point (Dirac point). The second experiment described graphene resistance change as a function of pH. Moreover, we also functionalised graphene by polyaniline to improve sensor qualities. We demonstrated pH sensitivity of graphene sensors on both substrates and discovered particular challenges regarding ionic strength, experiments themselves and graphene destruction.

KEYWORDS

graphene, parylene C, SiO_2, electric double layer, pH, ionic strength, polyaniline

ABSTRAKT

Pokrok ve vývoji nanotechnologií nám poskytuje dobrou příležitost k vývoji nových špičkových zařízení. Tato práce si klade za cíl vyrobit, popsat a změřit grafenové pH senzory na dvou různých substrátech - polymeru parylenu C a SiO2. Tento pH senzor je prvním krokem ve vývoji nositelné náplasti monitorující stav kůže a možné infekce. Grafen je 2D materiál na bázi uhlíku se zajímavými vlastnosti a nadějnými aplikacemi. Úspěšně jsme provedli dva různé experimenty sloužící k charakterizaci grafenových senzorů a jejich odezvu na různé hodnoty pH. V prvním experimentu jsme použili horní elektrolytické hradlo k určení bodu neutrality (Diracův bod). Druhý experiment popsal změnu rezistence grafenu jako funkce pH. Dále jsme také funkcionalizovali grafen polyanilinem, abychom zlepšili jeho vlastnosti. Prokázali jsme citlivost grafenových senzorů na pH pro oba substráty a objevili jsme několik výzev jako potřebu kontroly iontové síly, experimentů samotných a destrukce grafenu.

KLÍČOVÁ SLOVA

grafen, parylene C, SiO_2, elektrická dvojvrstva, pH, iontová síla, polyanilin

TRIPSKÝ, Andrej. *Design, fabrication and testing of graphene biosensors*. Brno, 2020, 62 p. Master's Thesis. Brno University of Technology, Faculty of Mechanical Engineering, Institute of Physical Engineering. Advised by doc. Ing. Miroslav Bartošík, Ph.D.

DECLARATION

I declare that I have written the Master's Thesis titled "Design, fabrication and testing of graphene biosensors" independently, under the guidance of the advisor and using exclusively the technical references and other sources of information cited in the thesis and listed in the comprehensive bibliography at the end of the thesis.

As the author I furthermore declare that, with respect to the creation of this Master's Thesis, I have not infringed any copyright or violated anyone's personal and/or ownership rights. In this context, I am fully aware of the consequences of breaking Regulation § 11 of the Copyright Act No. 121/2000 Coll. of the Czech Republic, as amended, and of any breach of rights related to intellectual property or introduced within amendments to relevant Acts such as the Intellectual Property Act or the Criminal Code, Act No. 40/2009 Coll., Section 2, Head VI, Part 4.

Brno ....

author's signature

ACKNOWLEDGEMENT

I cannot thank enough my Erasmus supervisor prof. Vincent Bouchiat who gave me the opportunity and introduced me to the topic of biosensors and was always willing to consult my countless questions. It is a pity that the coronavirus lockdown interrupted additional internship and I could not study the topic even more profoundly as I planned. My thanks also go to dr. Riadh Othmen who fabricated graphene sheets for me and was like a buddy for me during my stay in France. Wider thanks go also to the Hybrid group at the Néel Institute in Grenoble who made my internship unforgettable.

I wish to acknowledge the support and great love of my parents and family, who gave me the possibility to study without any troubles and encouraged me to study abroad. I did not have any doubt about their eternal support even for a blink of second and this gave me the peace of mind to finish the studies. Díky, mami a tati!

I would like to pay my special regards to my brother dr. Matěj Tripský and Anna Březná who were willing to proof-read my thesis and made it much better. Also, thank you, Anna, that you helped me to endure the beginning of the studies which were the most difficult and I had nearly failed if there was not your care and support.

I am indebted to my classmates who created a special, safe and funny environment. Thanks to this, I was always looking forward to the classes and all the university activities. Special thanks go to Jakub Piastek and Vojtěch Švarc for technical support during my studies and the work on the thesis. Not a smaller thanks go to Jan Tesař who was willing to measure Raman spectra with me cheered me up during writing of the thesis.

I would like to recognize the invaluable assistance of my supervisor dr. Miroslav Bartošík who allowed me to work on the topic I am so genuinely interested in. Thank you for all the consultations during Master, and also Bachelor studies and encouraging me with new ideas.

Contents

Introduction **1**

1 Theory **3**
1.1 Sensors . . . 3
1.1.1 Sensor properties . . . 4
1.1.2 Transfer function . . . 6
1.1.3 Types of sensors . . . 7
1.2 Biosensors . . . 8
1.2.1 Transducers . . . 10
1.3 Materials . . . 10
1.3.1 Carbon allotropes . . . 10
1.3.2 Substrates . . . 16
1.4 Electric double layer (EDL) . . . 18
1.4.1 Helmholtz model . . . 18
1.4.2 Gouy-Chapman model . . . 18
1.4.3 Stern model . . . 18
1.5 State of the art . . . 22

2 Experimental part **25**
2.1 Materials . . . 25
2.1.1 Sensor description . . . 26
2.2 Experiments . . . 26
2.2.1 Resistance on time dependency . . . 27
2.2.2 Resistance on gate voltage dependency . . . 28
2.3 Resolved challenges . . . 31
2.4 Buffer preparation . . . 32
2.5 Results . . . 34
2.5.1 Graphene on parylene C . . . 34
2.5.2 Graphene on SiO_2 . . . 39
2.5.3 Results summary . . . 47

Conclusion **51**

Bibliography **53**

List of abbreviations **61**

Introduction

The thesis focuses on the study of biosensors based on graphene, which is a material widely studied by the scientific community. The current trend of miniaturisation in most areas of technology allows us to use devices in yet unknown scale. Sensors are an excellent example. These devices are devoted to obtain relevant information about the environment. Furthermore, these data can be processed and evaluated for our needs.

In the thesis, we are going to fabricate, develop and describe such sensors.

First, we introduce the theory of biosensors and describe graphene we used as a sensing part. We apply various solutions on the graphene surface forming a thin interfacial electrolytically-active region called electric double layer (EDL). It has some interesting properties and its theory will be introduced.

We want to use our biosensor in the life science area. Therefore, the primary purpose is to obtain valid data from our body (from the skin to be exact). It is a pioneering step to develop device able to monitor skin wound condition such as a healing process and local infections. It can be a huge success for chronic wounds treatment. Chronic wounds are not healing wounds often affecting elderly people and diabetics. They are a serious problem and can even lead to limb amputation. One of the main problems is untreated infection or inflammation in the wound [1]. Therefore, our goal is to monitor the wound healing process and we chose pH as a measured variable. The reason is that pH is relevant to wound healing process. Thus, the focus of the thesis is the development of pH sensors based on graphene.

The first part of the experimental chapter describes the design and single parts of pH sensors. The second part is focused on studying a resistance response of sensors on pH with and without gate voltage assistance. The graphene sensor response is investigated on both parylene and silicon dioxide substrates. The results from the experiments are presented and discussed in the final part.

1 Theory

First, we have to look at the sensor's overview and its general principles to understand the background and drawbacks of the whole thesis. Then, we will focus on the materials used for our devices because they have some unique properties that will be discussed.

1.1 Sensors

There are many different definitions and descriptions of sensors. The very interpreting one is

"A sensor is a device that receives a stimulus[1] and responds with an electrical signal." [2]

This definition is comprehensive, but it is indeed describing the primary function of sensors. The typical idea might be that sensor is a human-made device consisting of sensing area and chip/computer able to send data further. Nevertheless, we have to think about it in the broader connotation. Living things are full of various sensors helping them to obtain data from its environment. These natural sensors are one of the underlying conditions for life systems as primitive as living cells. Cells and other life systems need to monitor environmental conditions and move towards better conditions if needed, and electrochemical reactions mostly drive these natural sensors [3]. These systems are a little bit different than human-made sensors as they do not have to convert stimulus into an electrical signal.
It is also important to distinguish between two very similar terms: *sensor* and *detector*. The main difference is that the detector is focused on qualitative measurement of the stimulus. It means that it gives us information if the stimulus is or is not present. On the contrary, the sensor is quantitatively focused, allowing us to know stimulus quantity and intensity. We can explain this better on a car example. Device verifying if doors are opened, or not is called a detector because it gives us only yes/no information. Whereas, a device measuring the distance from another car by e.g. infrared radiation, is called a sensor.

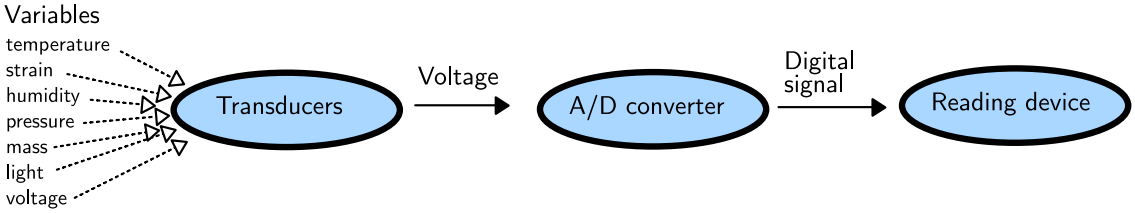

Fig. 1.1: Schema of the typical sensor. Adapted from [4].

[1] Stimulus is quantity, property, or condition that can be converted into a signal.

We have to distinguish between another two similar terms *sensor* and *transducer*, Fig. 1.1. The transducer converts one type of energy into another. Such as conversion of electrical energy into magnetic energy, mechanical into magnetic and others. The sensor is converting the signal always into electrical energy. Both transducers and sensors are used together in more complex systems. For example, transducers can transform motion energy into heat energy, and the sensor is then converting heat energy into electrical energy.
The human-made sensors are mostly simple devices with a known response to the observed stimulus. More sophisticated systems are made of many sensors which are controlled and synchronised by a computation unit. Sensors have different input signals based on what they measure, transforming this signal into an electrical output form. Transformation is a fundamental process because we can read the sensor's output signal with various electronic devices. Such devices are usually PCs, phones or embedded computer platforms (microcontrollers[2], systems-on-chips). Most of the sensors are not energy, size demanding and especially the possibility of using them with embedded computers is getting popular recently.

1.1.1 Sensor properties

The sensor is a data acquiring system collecting information about the environment and various stimuli. Future steps and functions of other systems are highly dependent on these data. Therefore, several important properties exist to describe the sensor and its quality. The work published by Skládal [6], gives us very nice overview which is further described in this section. For each property, we are trying to explain two different states: ideal and real.

Sensitivity

Sensitivity is defined as a measurable signal change ΔS on a change of stimuli concentration Δc. In case of kinetic measurements, sensitivity is $\Delta(\mathrm{d}S/\mathrm{d}t)/\Delta c$, see Fig. 1.3a. Sensor sensibility should be ideally constant in the sensor's lifetime, but it is not the real case and recalibration is needed.

Calibration

Calibration is done by measuring known standardised stimuli and adjusting the sensor's parameters. Again, the ideal case is to make one calibration after the production of the sensor. However, we need to do periodical recalibrations.

[2]Based on the comprehensive book written by McEwen [5], microcontrollers (Arduino, Texas Instruments, BeagleBone) are small devices with low energy consumption. Main parts are the processor, storage and RAM. Microcontrollers can be programmed to read data, process and send them back to the system or other devices. In recent years, microcontrollers are used more and more in various fields, mainly due to lowering its price. Thanks to this, many amateurs can create simple smart devices using sensors and microcontrollers and give "life" to many static things. Moreover, we can connect such devices to the internet, which is becoming frequently used and this trend is called the Internet of Things (IoT). A lot of such devices is using sensors (proximity, movement, light, touch). From this point of view, we can expect increased utilisation of a combination of various sensors and microcontrollers connected to the internet as shown in Fig. 1.2.

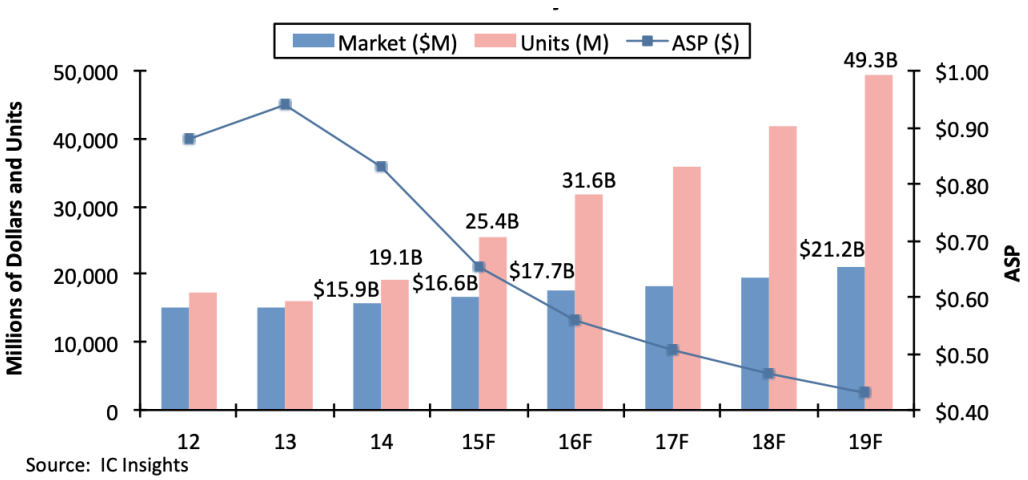

Fig. 1.2: Microcontrollers market. ASP - average sell price [7].

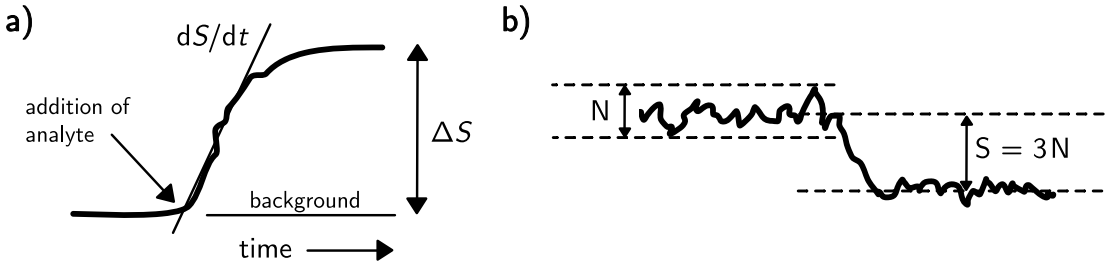

Fig. 1.3: a) Possible sensor response after the application of analyte. S is sensed value. We can measure stimulus both by change of S in time - dS/dt (kinetic measurement) or by reading saturated steady value ΔS [6]. b) Noise N and limit of detection $\frac{S}{N} = 3$

Linearity

If we want to read data from the whole measurement space, which is the goal for each sensor, $\Delta S/\Delta c$ should have the same dependency in the whole measurement space. It would allow us to read all values with one sensor. Real sensors have a narrower measurement area and are prescribed for a specific value range. Linearity makes calibration easier as we need only two points. Nonlinearity is mostly caused by saturation of the recognition part of the sensor. In some cases, we can linearise nonlinear response by logarithm. For example, the semilogarithmic conversion is used in potentiometry.

Limit of detection (LOD)

Limit of detection (LOD) is the lowest readable stimulus value. LOD is dependant on device measuring stimulus and is defined by noise ratio (N). LOD is often counted as $\frac{S}{N} = 3$, see Fig. 1.3b.

Noise

Noise is present in every electrical measurement. It is mostly electromagnetic origin from electricity which is operated on frequency 50 Hz. It is possible to lower noise using various electrical components or techniques (lock-in amplifiers, filters, averaging, smoothing).

Background

The signal without the existence of analyte is the background. Mostly, it is a constant value and we can deduct it from the measured signal:

$$S = S(\text{measured}) - S(\text{background}) \tag{1.1}$$

. Another approach is to use reference value:

$$\frac{S}{S(\text{ref})} = \frac{(\text{measurement} - \text{background})}{(\text{reference} - \text{background})} \tag{1.2}$$

Hysteresis

Hysteresis is the influence of previous measurements on current measurement. Ideally, it is zero. Reasons for hysteresis can be various, e.g. high analyte concentration affecting recognition layer, local differences in temperature, static charges and other. Hysteresis can be lowered by slower measurements and pauses between single measurements.

Biocompatibility

When the sensor is not affecting living tissues or cells it is biocompatible. It is crucial for biomedical applications as it should not cause any inflammation, swelling or blood poisoning.

Other

There are a few more properties suitable for a description of sensors. *Long-term stability* - low change of the sensitivity in time. *Selectivity* - selectiveness only to a specific substance. *Response time* - is the time needed to acquire the specified value of a signal, e.g. 95 % of the signal stable value. *Lifetime of biosensor* - is defined by the lifetime of the weakest part of the sensor. We also need to distinguish between the storage and the working lifetime.

1.1.2 Transfer function

Most stimuli do not cause a direct electrical signal of the sensor and must be more frequently transduced. These input-output relations need to be found and known. *Transfer function* transforms the input signal into the output signal which we read as the stimulus value.
The transfer function represents relationship between stimulus s and the measured

electrical signal E, $E = f(s)$. We need to use inversed function to discover real stimulus value s by $E = f^{-1}(s) = F(E)$. This function is ideally the same throughout the whole lifetime of the sensor. Unfortunately, the function is changing in time as it is not only dependent on the sensor alone but on all device components. The function has often not the same dependency in the complete range of stimulus. This often leads to a restriction of measurable values. The dependency of the transfer function should stay stable in time and only recalibration should be adjusting its parameters.

1.1.3 Types of sensors

Sensor by its definition is a broad term including many different devices. Therefore, we need to define subcategories which are selected by different criteria.

Energy source

All sensors can be differentiated by its external energy source on *active* and *passive*. Passive sensors do not have any additional external energy source and their functions do not need to be triggered or excited. It changes the signal based on the measured stimulus. For example, a photodiode or piezoelectric sensor are passive sensors.
On the contrary, active sensors require external excitation to measure stimulus. Sensors are not converting energy from the stimulus by themselves as in the case of passive sensors. Many stimuli causes a change of active sensor's material properties. Such change can be recognized by excitation signal. An excellent example is a thermistor. The thermistor changes its properties due to a different temperature. At any time, we use excitation signal and measure the resistance of thermistor which can be converted by the transfer function into observed value.

Characteristics and properties

Sensor's characteristics and properties allow us to group sensors into various categories. Let us mention some we can use to distinguish sensors.

1. **Sensor specifications** - sensitivity, stimulus range, stability, resolution, hysteresis, linearity, etc.
2. **Sensing element material** - inorganic, organic, insulator, conductor, semiconductor, biological substance, etc.
3. **Conversion phenomena** - physical (thermoelectric, photoelectric, electroelastic, etc.), chemical (chemical transformation, physical transformation, spectroscopy), biological (biochemical transformation, effect on test organism, spectrocopy, etc.)
4. **Field of application** - agriculture, automotive industry, energy power, medicine, military, etc.
5. **Stimuli** - acoustic (wave amplitude, wave velocity, etc.), biological, electric, magnetic, optical, mechanical, etc.

1.2 Biosensors

In the previous chapters, we gave a general overview of sensors and their properties. Typical sensors transduce signals into digitally readable form. Most of the measured variables describe the state of the environment (such as temperature, humidity, pressure, etc.). The interest of this thesis lies in *biosensors*.
Biosensors are sensible to the concentration of specific analytes, such as specific proteins, nucleic acids, compounds, bacteria and many more. Its usage is in many areas like food and water processing, monitoring, safety, metabolic engineering, biodefense and mainly healthcare industry which covers the biggest part of the biosensors market. Good example is a blood glucose meter which is essential for diabetics (85 % of the whole biosensor market [8]) or sensing of various pathogens [9]. For such specific analytes, we can not use only transducers as in previous sensors, but we have to use an additional component called *bioreceptor* [4].
Bioreceptors are biological compounds such as enzyme, antibody, nucleic acid, bacteria, which are specifically binding a target analyte and causing the transducer to generate a voltage which we can measure. The notable attribute is that biosensors are very specific thanks to the bioreceptors. First attempts of biosensors were based on the enzyme, which was used as a biorecognition layer for the glucose sensor. The enzyme is a protein that acts as a biocatalyst and is always bound to a specific substrate molecule, creating a new one. This binding is highly specific and analogous to the key and lock system as we can schematically see in Fig. 1.4. The more detailed biosensor description with specific examples is shown in Fig. 1.5.

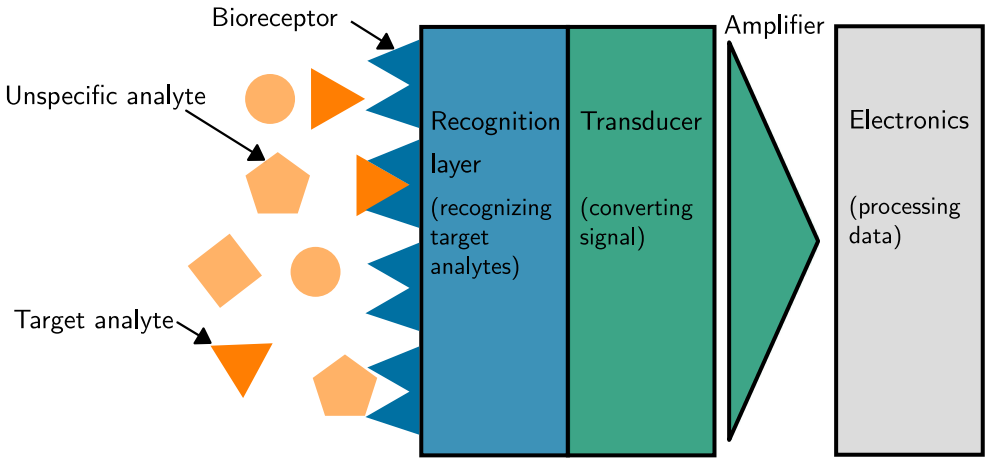

Fig. 1.4: Description of biosensor and specific binding.

For the glucose sensor, bioreceptor is an enzyme glucose oxidase (GOx) which is capturing glucose molecules. Functionalisation with GOx is very successful and such biosensors report good stability, linearity and low interference with other analytes [10][11][12]. Another interesting fact is that H_2O_2 is co-product of glucose and GOx reaction, so an indirect method by observing the concentration of H_2O_2 and recalculating it on glucose concentration can also be used. In fact, one of the first

glucose sensors were such a type [13][14].
Very similar to enzymes as bioreceptors are antibodies which are protein molecules responsible for immune system response. Antibody is selective only to a specific protein molecule called *antigen*. Such system is mimicking immune system and is often called an *imunoassay system* [15][16].
Another often used bioreceptors are nucleic acids DNA and RNA. As we know, they consist of four different bases: adenine (A), thymine (T), guanine (G), cytosine (C) for DNA and adenine (A), uracil (U), guanine (G), cytosine (C) for RNA. Nucleic acids are long chains which consist of these four bases in various combinations. The important fact is that each base has exactly one anti-base - A-T, C-G for DNA and A-U, C-G for RNA. Such limited compatibility gives us a great tool to "code" bioreceptors. We can use a specific sequence of nucleic acid as bioreceptor and it will be sensitive only to the nucleic acid to which it is set up to. Once again, we have something similar to the key and lock system. The longer the sequence is, the more stable and accurate bioreceptor we have as we lower the possibility of interference with different nucleic acids or errors in the sequence. Nucleic acids as bioreceptors are essential in recognition of various viruses and bacteria [17][18][19].

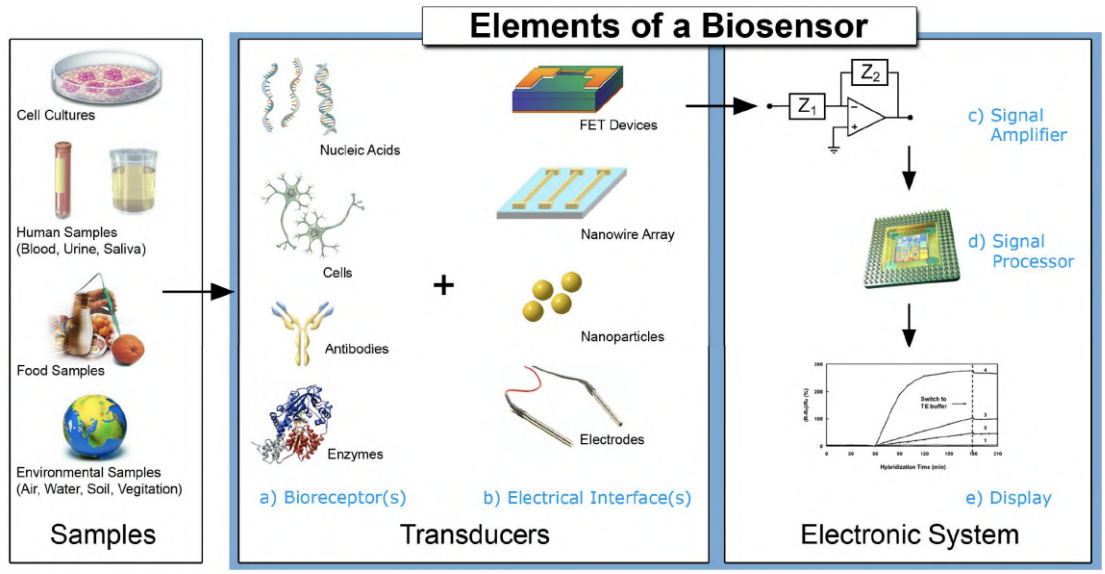

Fig. 1.5: Schematic description of element order in the typical biosensor [20].

For biosensor fabrication of the desired quality, some criteria need to be met [8][20]:

- The desired analyte should be specific and stable under storage conditions.
- The sensor should be accurate, precise, and show high sensitivity in a reproducible way, and linearity with different concentrations.
- Physical parameters such as pH, the temperature should be optimised, which assures analysis with minimal pretreatment.
- The biosensor should be biocompatible.
- The fabricated biosensor should be small, portable, cost-effective and capable of being used by semi-skilled operators.

- The biosensor should provide a real-time analysis so that it can be used for rapid measurements of analytes from human samples.

1.2.1 Transducers

Paramount part of each biosensor is a transducer which converts the signal from the biorecognition layer into a readable form, mostly voltage. Proper choice of the transducer is essential, especially because various bioreceptors are used in biosensors. There are more types of transducers utilised in biosensor devices and each has its specifications.

Electrochemical

Probably most common biosensor's transducers are electrochemical. The basic principle is that reaction between the target analyte and bioreceptor creates or absorbs ions or electrons. The electrochemical signal is then quantitatively related to the amount of analyte. The exact relation is based on the transfer function of the device. Different quantification methods are used, such as potentiometry, amperometry, voltammetry and electrochemical impedance spectroscopy.

Optical

Another much more diverse group of transducers used for bioreceptors are optical transducers. Many different types of spectroscopies can be used, such as absorption, fluorescence, Raman, phosphorescence, refraction and dispersion. In optical transducers, many parameters describing a light wave, such as amplitude, phase, polarisation, energy, decay, can be used. Optical transducers are often used for measuring an analyte concentration which influences light wave function parameters [22].

1.3 Materials

1.3.1 Carbon allotropes

Carbon is very common atom which can be found in all organic molecules and exists in many different forms (allotropes), Fig. 1.6a. Graphite and diamond are the best known forms, however, we are not going to study them further here.

Fullerenes

More recent carbon allotropes are fullerenes which were synthesized in 1985 by a team at Rice University, lately awarded by Nobel Prize in Chemistry in 1996 [23]. Most common fullerenes are like a football ball (buckyball) looking molecules consisting of 60 carbon atoms (C_{60}). Fullerenes with different number of carbon atoms

were described as well C_{24} [24], C_{36} [25], C_{70} [26] and many others.

Carbon nanotubes (CNTs)

Another impressive allotrope is a carbon nanotube (CNT). It shares some of the features with fullerenes. Moreover, they should be mentioned in the same context because while producing buckyballs in the 1980s, there were observed needle-shaped structures which were carbon nanotubes. The first image of carbon nanotube was published in 1959 by Roger Bacon. In the 1980s, Howard Tennant applied for a patent dealing with a production of CNTs, but the real discovery was credited to Sumio Iijima in 1991 [27]. Carbon nanotubes have cylindrical shape consisting of single/multi-wall layer of carbon atoms (graphene). Structure of fullerenes is compatible with nanotubes, so half of the fullerene can be used as a cap. Nanotubes have a small inner diameter ranging from 10 Å to 30 Å and are considered as carbon 1D system. Most of the theoretical work is done for single-wall CNTs which makes it difficult to verify experimentally. It is very challenging to produce single-wall nanotube of a given diameter and measure it accurately. Progress was achieved in the research of CNTs, e.g. scanning tunnelling spectroscopy described the CNT's electronic density of states or transport measurements were performed by contacting CNTs with golden electrodes using lithography [28].

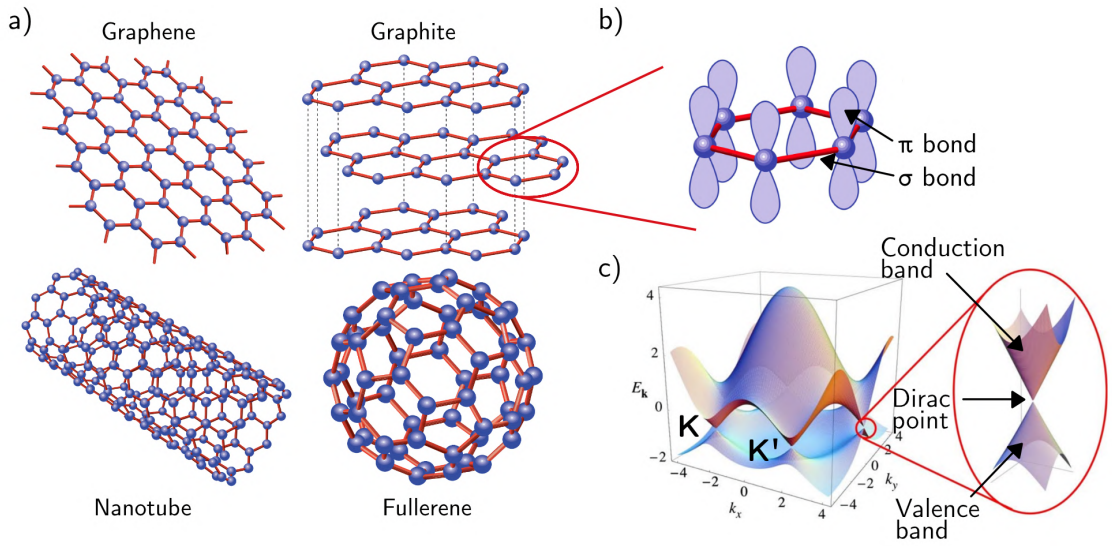

Fig. 1.6: Selected carbon allotropes and graphene electronic properties. a) Four carbon allotropes, all formed in a hexagonal lattice. Graphite is a structure consisting of graphene multilayers bonded by van der Waals force. b) Orbitals of the single hexagonal lattice. c) Band diagram of graphene [29][31].

Graphene

The most recent carbon material is graphene which has received a lot of interest from scientist from various fields of study. It was isolated in 2004 by Andre Geim

and Konstantin Novoselov who were awarded for this discovery by the Nobel Prize in Physics in 2010 [32]. It is a one atom layer thick material with carbon atoms arranged into a hexagonal lattice (honeycomb). Due to its structure, it has some properties making it an extraordinary and promising material for electronic and sensing applications. It has also a high thermal conductivity $\sim 5000\,\mathrm{WmK^{-1}}$ [33], gas impermeability [34] and light transmittance $\sim 97.7\,\%$ [35]. Mechanical and electronic properties will be described in detail.

Mechanical properties

Graphene has carbon atoms with spacing $a = 142\,\mathrm{pm}$ (δ_i in Fig. 1.7). Stable sp^2 bonds forming hexagonal lattice oppose many in-plane deformations. Lee et al. studied intrinsic strength and elastic properties of graphene using Atomic Force Microscopy (AFM) nanoindentation and discovered Young's modulus $E = 1.0\,\mathrm{TPa}$, which corresponds to by their words "the strongest material ever measured" [36]. It is important to highlight that this high material strength is determined for defect-free graphene and in-plane direction. Other reports discovered lower values which are attributed to crumpling and wrinkles in the out-of-plane direction. Therefore, we need to be more reserved when describing the strength of this 2D material. A very nice analogy can be found in a bedsheet which is relatively stiff in in-plane direction but it can be easily folded and bent.
Fracture toughness is more important for engineering applications. The fracture toughness of graphene was determined by creating artificial cracks using a focused ion beam (FIB). The same as for the other materials, the material failure was initiated around the crack. The fracture toughness was measured as a critical stress intensity factor $K_\mathrm{C} = 4.0 \pm 0.6\,\mathrm{MPa}$ [37]. Many parameters describing graphene properties are calculated for pristine graphene. This research [38] found a close relation between polycrystalline graphene grain boundaries size and its fracture toughness. Fracture toughness was discovered to be 20-35 % higher than the one of pristine graphene, and the explanation lies in larger energy release rates. Moreover, decreasing grain size causes an increase in energy release rates. This can help us to control the toughness of graphene when producing it by chemical vapour deposition (CVD), which will be discussed later. Grain size can be controlled by changing parameters in CVD growth [39].

Electronic properties

Electronic properties are maybe even more fascinating than mechanical. Each carbon atom has four valence electrons. Three of them are arranged into sp^2 hybridized orbitals forming strong equivalent σ-bonds with 120° angle. The fourth orbital is perpendicular to others creating π-bonds, Fig. 1.6b, and this electron is dissipated forming so-called *free electron cloud*. The bonds in z direction are weaker (van der Waals). It also explains the theory behind writing with a pencil. The pencil is formed from graphite which are basically layers of graphene on top of each other bonded by van der Waals forces, Fig. 1.6a. As we write, we are breaking these bonds and leaving multilayers on paper. Graphene was discovered by the same principle. Adhesive scotch tape was used to release layers of graphene from graphite

and imprinted on the substrate. This process was repeated until the monolayers were present.

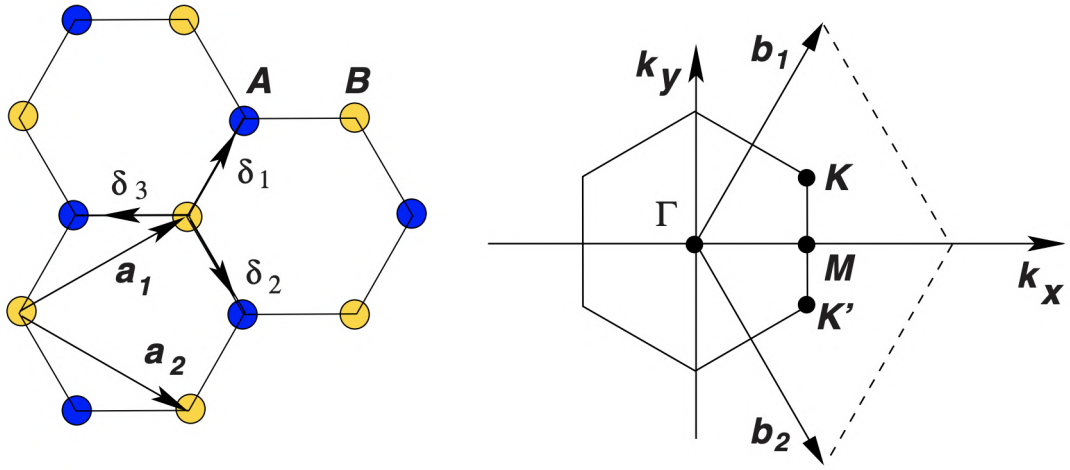

Fig. 1.7: Honeycomb graphene lattice. Left: Lattice structure from two triangular lattices. $\boldsymbol{a_i}$ are lattice unit vectors and $\boldsymbol{\delta_i}$ are nearest-neighbour vectors. The unit cell contains two atoms. Right: Brillouin zone with important points K and K', which we call Dirac points and are also illustrated in Fig. 1.6c [31].

The band structure in K and K' points (Dirac points) is appealing because of the behaviour of the charge carriers. Fermi level lies in the crossing point between cone shaped dispersion relations representing conduction and valence bands. From this point of view, graphene is considered as a zero band gap semiconductor [30] or by some reports metal [40]. Moreover, when we calculate energy ϵ at this point, which is given by $\epsilon(\boldsymbol{k}) = \pm\hbar v|\boldsymbol{k}| = \pm v|\boldsymbol{p}|$ for small $k = |\boldsymbol{k}|$, where $\boldsymbol{k}$ is the wave vector, $\hbar$ is reduced Planck constant, $\boldsymbol{p} = \hbar\boldsymbol{k}$. Based on the special theory of relativity, the energy of relative particle is $\epsilon = \sqrt{m^2c^4 + c^2\boldsymbol{p}^2}$. If we set $m = 0$, we obtain dispersion relation $\epsilon = c|\boldsymbol{p}|$. This is a mas-less particle neutrino and if we substitute c with v, we have energy dispersion relation for electron in graphene. It means that electron is behaving like mass-less particle in graphene and CNTs, which is giving it outstanding electronic properties.
The conductivity is the lowest when the Fermi level E_F crosses Dirac point. The theory also predicts that conductivity should be independent on electron concentration, which is not verified experimentally. Experimentally is conductivity nearly proportional to the electron concentration [40]. The scatterers such as charged impurities are one of the reasons for this dependency. Explicit calculations later show dependency $W \propto |n|^{-1}$, where W is a dimensionless parameter characterising the strength of impurity scattering. Conductivity is then derived from the Drude model as $\sigma \approx e|n|\mu$, where μ is mobility independent on n. Typical values on SiO_2 substrate are $\mu \approx 10^4\,\mathrm{cm^2V^{-1}s^{-1}}$ and the impurity concentration $n \approx 10^5\,\mathrm{cm^{-2}}$ [41].

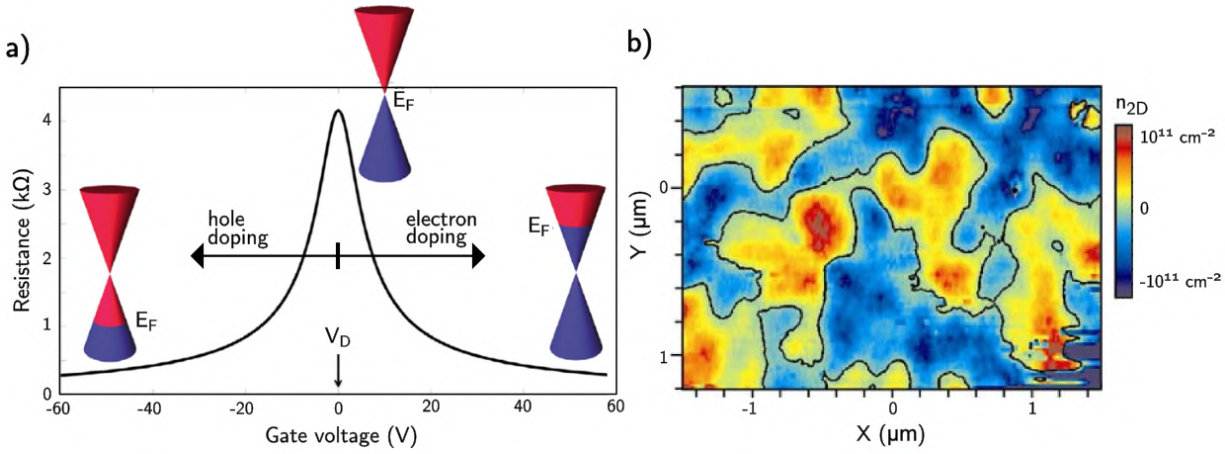

Fig. 1.8: a) The typical dependency of resistance R on applied gate voltage V_g. The highest resistance value is at Dirac point V_D. At this point, the number of carriers is at equilibrium and the lowest. Thus, R is the highest. Gating in both directions is shifting Fermi energy E_F and in the negative values from V_D is graphene electron-doped (n-doped) and in the opposite direction, hole-doped (p-doped). The real samples have only rarely V_D exactly at $V_g = 0\,V$ due to impurities, lattice deformations, substrate doping, contacts, etc. Adapted from [42]. b) Colour map of the spatial density variation of graphene flake. Blue region corresponds to holes and red to electrons, local doping caused by electrons [43].

Graphene doping

Unusual zero bandgap and linear function at K and K', see Fig. 1.7, allow us to tune graphene electronic properties. The pristine graphene should have Dirac point $V_D = 0\,V$, which is not true for real graphene samples. Graphene is basically only 2D material and it is very susceptible to foreign atoms and molecules. It can be electrostatically doped by its absorbates from both sides (surface and substrate). This doping is random and localised. Finally, graphene surface doping is not uniform but is localised forming "electrostatic puddles" of p or n doping. The puddles could be the reason why graphene never has zero conductance, since there are always localised doped areas, see Fig. 1.8b.
To sum up, we have two primary sources of graphene doping. First one is intrinsic doping from graphene structure, substrate and adsorbed atoms or molecules. This is ideally constant value characterising the graphene sample. On the other hand, in the experiments, external doping is produced by gating and consequent field effect. We can find the Dirac point by observing resistance dependency on a gate voltage, see Fig. 1.8a. Graphene can also be externally doped by various ions changing surface static charge, which will be studied in this thesis.

Graphene fabrication methods

There are a lot of fabrication and transfer methods of graphene. Let us focus on them and describe two main methods. Graphene was discovered by exfoliation from

graphite, which will be briefly introduced. Larger sheets and scalable production can be achieved by chemical vapour deposition (CVD).

Mechanical exfoliation

Mechanical exfoliation was used by Geim and Novoselov in 2004 [32],and led them to the Nobel Prize in Physics in 2010. The method is straightforward, but at the same time, produces the highest quality graphene. A thin layer of graphite is pulled by scotch tape from the pure graphite flakes leaving grey piece on the scotch tape. Now, another part of scotch tape is used to make the layer even thinner. This process is repeated a dozen times after which the last part can be put on the substrate (mostly SiO_2).
The advantage of this method is its simplicity since we do not need any special equipment. At the same time, the graphene "fabricated" by this method has the highest quality and electron mobility. A disadvantage is that it is not rigorous, fully-controlled method. The number of needed repetitions and the outcome are varying as it is challenging to apply always the same pressure and have standardised conditions. Fabricated flakes have various sizes in the order of µm. This type of method is often used in fundamental research since it gives us the highest quality and the small size of flakes is not an obstacle, because we mostly do not need to cover large areas.

Chemical vapour deposition (CVD)

This technique of catalytic growth is a promising candidate for large-scale, cost-efficient production, which is needed if graphene should be applicable in modern, daily-life devices.
CVD growth is based on growth on the substrate serving as a catalyst. Such substrate is mostly copper Cu or nickel Ni. Carbon atoms forming graphene are extracted from carbon-containing gases such as methane or acetylene [44].
Exact parameters for each growth are a little bit different. This study [45] reported catalyst growth on copper foil 25 µm thick. The whole process of catalytic growth can be seen in Fig. 1.9a. First, the copper foil is heated under low pressure with the atmosphere of H_2. Sometimes annealing by argon is also used, which smoothes copper foil and diminishes surface inequalities. After the preparation, methane is injected into the growing chamber. Methane molecules are broken under such conditions and carbon atoms are captured on copper foil surface. In a short time, the crystal centres are created and the growth is continuing around them. These grains are expanding their diameters until they get in contact with other grains. These borders are called grain boundaries and have different properties than the rest of the graphene. Size of grain boundaries is dependent on growth parameters and is one of the parameters used for the description of CVD graphene.
Sometimes a multilayer is formed in the centres where growth started. This can happen if the growth is too fast. Appealing advantage of this technique is self-determination. Once the copper foil is covered with graphene, the growth is stopped. This helps in achieving such excellent outcomes that $\sim 95\,\%$ of the copper foil is

covered with a graphene monolayer and the rest with two or three layers [45].

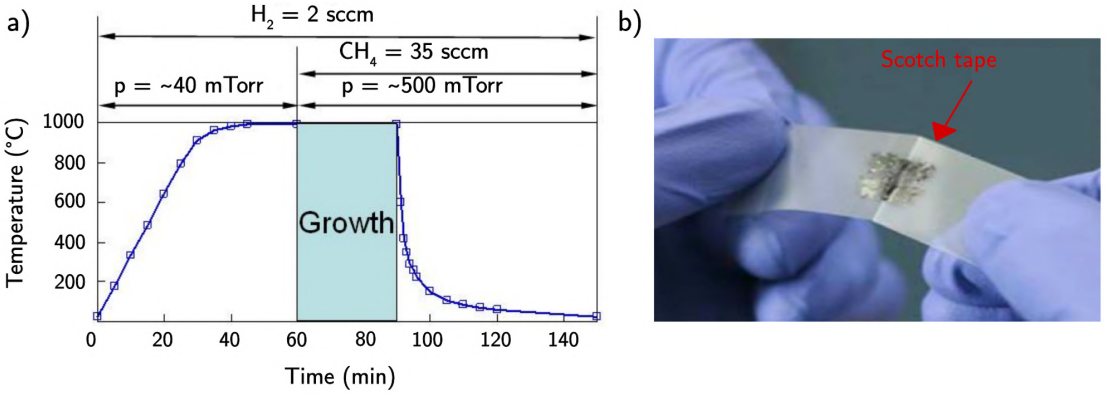

Fig. 1.9: a) The CVD growth process [45]. b) Exfoliation using scotch tape [46].

1.3.2 Substrates

A copper foil is only the catalyst and we need to transfer graphene on the desired substrate because it is not a self-standing material.

SiO_2

Such substrate is mostly silicon wafer with SiO_2 on the surface. Silicon wafers with SiO_2 are widely used in research and we are not going to describe them in detail here. It is worth mentioning the transfer process from the copper foil on the silicon substrate. It is done in this order

1. Poly(methyl methacrylate) (PMMA) is spin-coated on graphene on copper foil.
2. Copper foil is etched by iron trichloride $FeCl_3$ or ammonium persulfate $(NH_4)_2S_2O_8$ [47].
3. Graphene on PMMA is transferred on the SiO_2.
4. PMMA is repeatedly bathed in acetone and water to remove PMMA and its residues.

Parylene

The second very important material for this thesis and not very well known is parylene C. It is a considerably different material compared to SiO_2. Parylene C [poly(dichloro-p-xylylene)] is a polymeric material mainly used as a substrate [48] or encapsulation material in life sciences [49], see Fig. 1.10. Letter "C" specifies the type of parylene because there are more types varying in structure bonded to benzene core, Fig. 1.11. It is transparent, biocompatible [50], chemically and biologically inert. It also functions as an electrical insulator.
Its fabrication and the form it can cover materials is very attractive for this material. Parylene C is available and sold in its dimer form. The dimer is vaporised and later

split by pyrolysis into monomers, see Fig. 1.12. These monomers are lead into the vacuum chamber with material that should be covered by parylene. Monomers are cooled down, attaching to the material and forming a polymer coating. The coating is 1 µm to 50 µm thick based on the deposition time [53].
Graphene on parylene production skips the step of using PMMA. Graphene on the copper foil is inserted into the chemical vapour deposition polymerisation (CVDP) chamber and covered by parylene. After that, the copper foil is etched, leaving only the graphene on parylene.

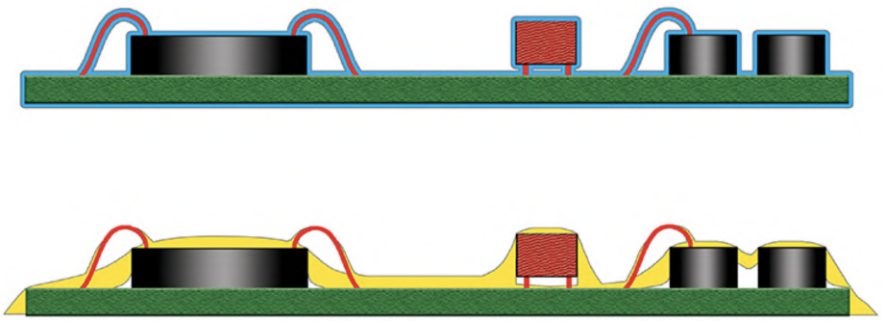

Fig. 1.10: Top: Parylene C uniform film covering all parts of device. Bottom: Liquid coverage of variable thickness and not covering whole device [52].

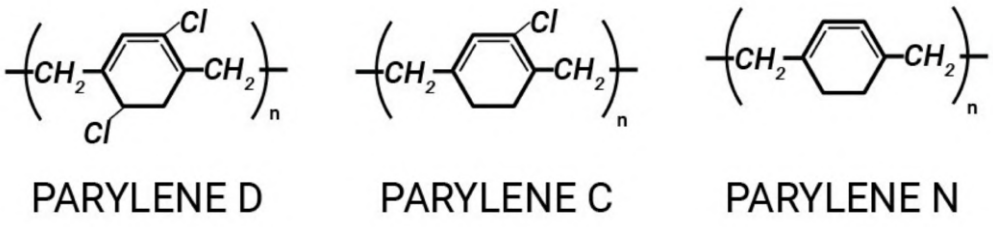

Fig. 1.11: Chemical structure of some selected types of parylene.

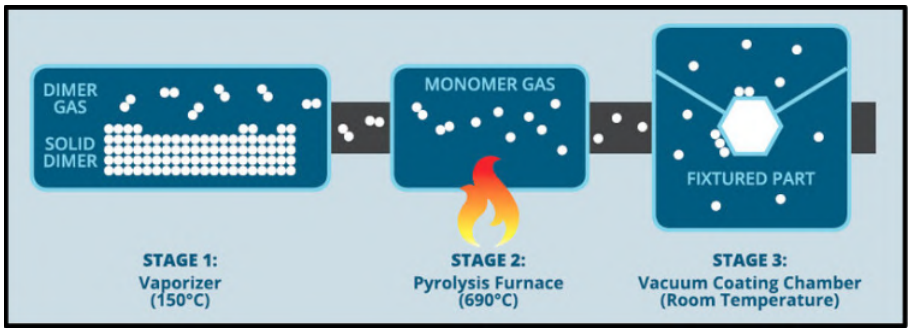

Fig. 1.12: Parylene C fabrication process using chemical vapour deposition polymerization (CVDP) process [53].

1.4 Electric double layer (EDL)

The critical section we need to describe in the theoretical part is a part of electrochemistry. It is describing potential distribution in the proximity of the electrode's charged surface and this section is mostly inspired by the 2nd chapter "The Electrified Interface" from the book [55]. Any surface in contact with electrode acquires charge which is different from that of the bulk solution. There are four ways how to acquire a charge at the surface:

1. Imposition of a potential difference from external potential source.
2. Adsorption of ions on a solid surface.
3. Electron transfer between the metallic conductor and the solution.
4. Biological macromolecules with ionisation of functional groups.

Surface charge effects are especially mattering in biological systems, where most of the reactions are realised in the proximity of surface.
Charged surface in contact with electrolyte solution attracts ions of opposite charge and repel ions of similar charge. Such a system is establishing an ion atmosphere near the surface area. Such configuration of two parallel systems of opposite charges is called the electric double layer (EDL). There are three main models describing EDL - *Helmholtz*, *Gouy-Chapman* and *Stern* model, Fig. 1.13.

1.4.1 Helmholtz model

Helmholtz model is the first and the simplest model describing contact between the liquid electrolyte and solid charged electrode. The model was introduced in 1871 [54]. The main assumption is that counter ions are immobilised establishing layer which is neutralising electrode surface charge. Surface potential Φ_0 is rapidly decreased to 0, see in Fig. 1.13.

1.4.2 Gouy-Chapman model

This model involves random thermal motion, which is the main difference compared to the Helmholtz model. Therefore, ions are not immobilised at the surface but are creating a diffuse double layer.

1.4.3 Stern model

Stern described that neither Helmholtz or Gouy-Chapman model is right on its own. He combined these models and made the assumption: some ions are immobilised at the surface (Helmholtz model) but not enough to neutralise electrode surface charge; rest of the charges is neutralised with the diffuse double layer from Gouy-Chapman model.
Mathematical description and derivation of the Stern model will give us a more profound understanding of ions and potential distribution near the contact between electrode and electrolyte.
The distribution of electric potential is described by *Poisson's equation*:

$$\nabla^2\Phi = -\frac{\rho}{\epsilon\epsilon_0} \tag{1.3}$$

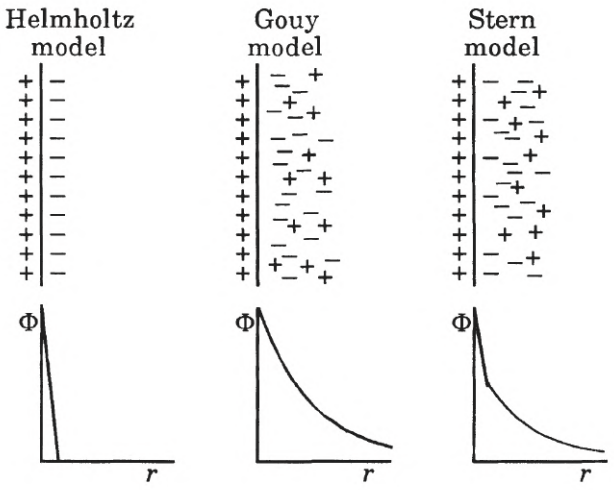

Fig. 1.13: Three models of electric double layer (EDL).

The space charge density ρ is described by ion charges and concentrations in solution by

$$\rho = \sum_i z_i F C_i, \tag{1.4}$$

where z_i is the charge of i ion, F is the Farraday constant[3] and C_i is the concentration of i ion.
We are able to obtain the relation between equations 1.3 and 1.4 but neither of these quantities is known. The link between these equations can be found with Boltzmann distribution law

$$\frac{N_1}{N_0} = \exp\left(-\frac{E_1 - E_0}{kT}\right), \tag{1.5}$$

which describes the ratio between N_1 particles with energy E_1 and N_0 particles with energy E_0. Variable k is the Boltzmann constant and T is the absolute temperature. Number of particles N_i gives the concentration of ions in the area with specific potential energy.
The electrostatic potential energy used in the previous equation is given by

$$E_i = z_i e \Phi. \tag{1.6}$$

Arbitrary zero of potential energy will be chosen as the electric potential energy of bulk in the solution with N_0 ions. With assumptions such as equation (1.6), N_i is proportional to concentration C_i and $e/k = F/R$, where R is molar gas constant, we can rewrite (1.5):

$$\frac{C_i}{C_i^0} = \exp\left(-\frac{z_i F \Phi}{RT}\right). \tag{1.7}$$

Finally, we can combine (1.4) and (1.7) and get result for charge density based on ions concentration

$$\rho = \sum_i z_i F C_i^0 \exp\left(-\frac{z_i F \Phi}{RT}\right), \tag{1.8}$$

[3] $F = 96\,485.332\,\mathrm{Cmol}^{-1}$

and we can substitute into *Poissons's equation* (1.3):

$$\nabla^2\Phi = -\frac{F}{\epsilon\epsilon_0}\sum_i z_i C_i^0 \exp\left(-\frac{z_i F\Phi}{RT}\right). \tag{1.9}$$

Solution of this differential equation ((1.9) *Poisson-Boltzmann*) gives potential distribution as a function of the position in the solution. The very illustrative solution of this equation is when we use expansion of exponential term into a power series. In such a solution, we will see terms that are important for this thesis and that are mentioned throughout it.

Solution of the Poisson-Boltzmann equation

Approximation of exponential equation is

$$\exp(-u) = 1 - u + \frac{1}{2}u^2 + \dots \tag{1.10}$$

and for the assumptions that $z_i\Phi \ll RT/F$, we can rewrite (1.9):

$$\nabla^2\Phi = -\frac{F}{\epsilon\epsilon_0}\sum_i z_i C_i^0 \left[1 - \frac{z_i F\Phi}{RT} + \frac{1}{2}\left(\frac{z_i F\Phi}{RT}\right)^2 + \dots\right] \tag{1.11}$$

The first term vanishes because the bulk solution is electrically neutral and we end up only with the second term and the equation looks like:

$$\nabla^2\Phi = \frac{F^2\Phi}{\epsilon\epsilon_0 RT}\sum_i z_i^2 C_i^0 \tag{1.12}$$

In this equation, we can substitute term which is used in electrochemistry and is describing the influence of ions in solution - *ionic strength* I defined as

$$I = \frac{1}{2}\sum_i z_i^2 C_i^0. \tag{1.13}$$

Thus, (1.12) can be rewritten

$$\nabla^2\Phi = \frac{F^2 I\Phi}{\epsilon\epsilon_0 RT} \tag{1.14}$$

and we obtain linearized Poisson-Boltzmann equation

$$\nabla^2\Phi = \frac{\Phi}{x_A^2}, \tag{1.15}$$

where x_A is constant representing the thickness of the ion atmosphere at the charged surface

$$x_A = \sqrt{\frac{\epsilon\epsilon_0 RT}{F^2 I}} \tag{1.16}$$

At given circumstances the solution in direction x perpendicular to yz plane, is as follows:

$$\Phi(x) = \Phi_s \left(1 - \frac{x}{a}\right) + \Phi_a \left(\frac{x}{a}\right) \qquad x < a, \tag{1.17a}$$

$$\Phi(x) = \Phi_a \exp\left(\frac{a - x}{x_A}\right) \qquad x > a. \tag{1.17b}$$

Where Φ_s is the surface potential, Φ_a is the potential at the Helmholtz layer defined by a. a is the thickness of the first part of the layer, immobilised Helmholtz layer. In this layer, the potential is linearly decaying, because we can simplify it by using two planes with different potential in the distance a which is nothing more or less than a planar capacitor. Outer layer solution (1.17b) for $x > a$ is equivalent to Gouy-Chapman diffusive layer and potential is exponentially decreasing.
Solution for the surface of a sphere is very similar.

$$\Phi(r) = \Phi_a \left(\frac{a}{r}\right) \exp\left(\frac{a - r}{r}\right) \tag{1.18}$$

It is not dependent on the angle but only on one variable - radial distance r.
The most important conclusion of this mathematical solution is the thickness of the EDL as a function of electrolyte solution's ionic strength. As was mentioned before, EDL can be simplified by a planar capacitor with thickness dependent on the ionic strength of the solution.
If we look at (1.16) we can see the x_A value is decreasing with higher ionic strength I. There is no direct measurement method of EDL thickness and we use calculations to describe such phenomena. More detailed overview of different cases is in Tab.1.1. It is good to keep in mind that ionisation does care too. For example, NaCl molecule ions are in ratio 1:1 (Na^+, Cl^-), $MgSO_4$ ions are in ratio 2:2 (Mg^{2+}, ${SO_4}^{2-}$). Even though the values are slightly different due to various conditions applied for calculations, we see two important facts.

Firstly, the thickness of the EDL layer is very small in the order of nm, see Fig. 1.14. This fact is causing higher capacitance of the system than of the systems we are able to create for back gating created in the silicon industry, where is the distance between electrodes ∼300 nm. Possibility of acquiring high capacitance at such low

Tab. 1.1: Calculated x_A values from two different references for ion concentrations $c = 0.1\,\mathrm{M}$ and $c = 0.01\,\mathrm{M}$, $1\,\mathrm{M} = 1\,\mathrm{mol} \cdot \mathrm{dm}^{-3}$. First calculation is for NaCl from [56]. The ratios are from different work [55] and represent ionization value z_i.

	x_A (nm)					
c (M)	NaCl	1:1	1:2	1:3	2:2	2:3
0.01	0.91	3	2.5	2.15	1.52	0.78
0.1	0.62	0.96	0.78	0.68	0.48	0.25

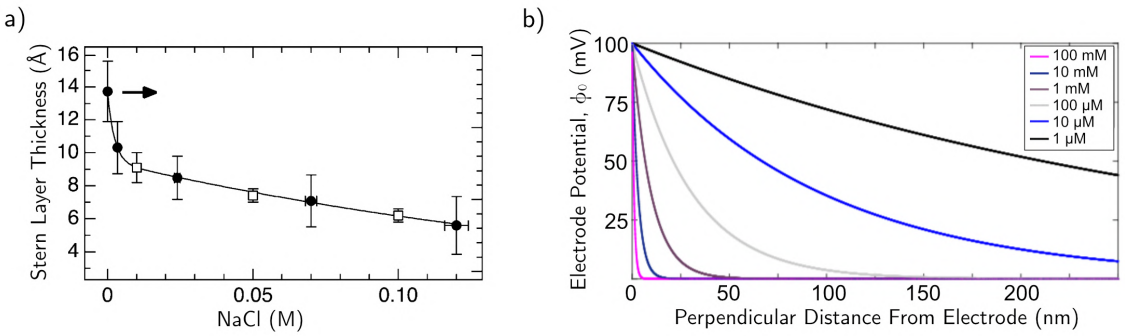

Fig. 1.14: a) Decreasing EDL thickness with increasing ionic strength of NaCl molecules, adapted from [56]. b) Potential decrease as a function of distance from electrode for various ionic strength. Significant drop is for higher ionic strength, adapted from [61].

thickness of the layer is used for many applications. Electric double layer capacitors (EDLCs) are promising candidates for the usage where needs to be stored a vast amount of energy and it is advantageous to save space. A promising application is energy recycling in vehicles where capacitors are charged during braking and the stored energy is used for acceleration. This technology still has drawbacks but its capacitance higher in range of magnitudes of the classic capacitors is making it a promising candidate for future applications [57][58][59][60].
Secondly, the thickness of the layer is decreased with higher ionic strength which is dependent on the concentration of C and the square value of the ionisation value z_i^2.

The Stern theory is a good approximation for more diluted electrolytes with the ionic strength up to 100–200 mM. For higher concentrations, the theory itself can lead to absurd values. The main problem is that the theory takes into account only the interactions between charged surface and ions in electrolyte but not ion-ion interactions. This is a sufficient approach when the electrolyte is diluted and the distance between ions is higher. For illustration, 1 M NaCl would give us concentration of bulk 47 M which means 30 ions per cubic nanometer.
Despite this drawback, the theory successfully explains many behaviours of colloids, nanoparticles in electrolyte solutions and other parts of electrochemistry. It is also used as the leading theory for top liquid gates and capacitors based on electric double layer. For more accurate calculations of EDL is the model supported by various computational methods [62][63].

1.5 State of the art

One of the most graphene's promising application is biosensing and there is a variety of articles written in this area.
Lei et al. [64] developed simple graphene pH sensor. The graphene was mechanically exfoliated on SiO_2 and no further functionalisation was used. Two platinum contacts were deposited on graphene and the gap between them had 200 µm–300 µm.

The article has reported a linear resistance decrease with increasing pH, which was tested in the range from 4 to 10. The highest measured sensitivity was 2 kΩ/pH.
Ang et al.[65] did the experiment with epitaxially grown graphene and discovered that OH^- and H_3O^+ adsorption dominated the electrochemical double layer. The experiment was focused on the Dirac point shift which increased with higher pH in the direction of positive voltage (p-doping). The shift was 98 mV/pH which is much higher than the theoretical Nernst limit 59.2 mV/pH. Such high Dirac point shift was discovered only for the negative voltage which may suggest that OH^- can be preferentially attached to the surface due to hybridisation between the unpaired electron of OH^- and the surface p-orbital.
Researchers from Delft University [66] did a broad study on single-walled carbon nanotubes (SWNTs) and graphene on SiO_2. They studied shift of Dirac point V_D based on various factors (concentration, type of salt, pH). V_D shift was dependent both on concentration and pH. Increasing concentration shifted V_D into negative values (n-doping graphene) and decreasing pH also shifted V_D into negative values, Fig. 1.15a. Salts LiCl and KCl had qualitatively same effect and it seems that important is only number of ions (concentration) and not type, Fig. 1.15b. The fact worth mentioning is a changed slope of dependency for pH = 3. The explanation given by authors lies in the device's isoelectric point pK_a, which is neutrality point and was determined by a computation to 4.5. The calculation counts with two types of ionisable groups with the opposite charge sign which is changed at pK_a.

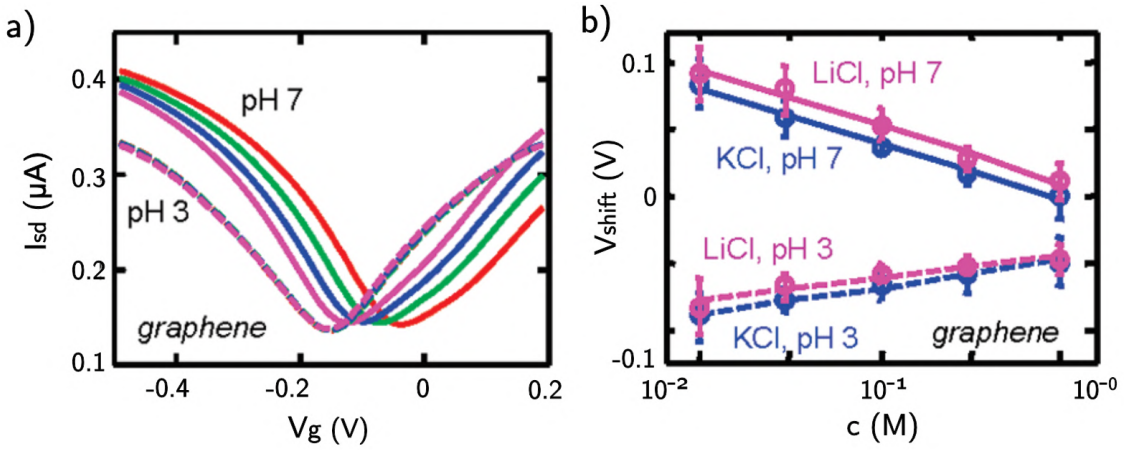

Fig. 1.15: a) I_{SD} on V_g curve for phosphate buffer. Dashed curves are for pH 3. Solid lines for pH 7 and the red, green, blue, and magenta curves were measured at 30 mM, 100 mM, 300 mM, and 1 mM KCl, respectively. b) Data averaged from 13 different graphene devices. Values are taken with respect to 1 M KCl, pH 7 curve. Adapted from [66].

A perfect example of broad graphene sensing capabilities showed Wang [67], who designed and measured device consisting of Ta/graphene wires. Ta wires 0.6 mm in diameter were covered by CVD graphene consisting of 1 to 10 monolayers (confirmed by Raman spectroscopy). Graphene was applied on clean Ta wires by high-power direct current arc plasma jet CVD. Differential pulse voltammetry (DPV) was used

for sensing ascorbic acid (AA), dopamine (DA), uric acid (UA), tryptophan (Trp) and nitrite (NO_2^-) in human serum, Fig. 1.16a. The limit of detection was 1.58 µM for AA, 0.06 µM for DA, 0.09 µM for UA, 0.10 µM for Trp and 6.45 µM for NO_2^-. The researchers conclude that graphene helped to increase the surface area of the electrode which facilitated ion adsorption and at the same time, high conductivity accelerated the ion diffusion and electron transfer. The device also had many edge defects which are considered as the most sensitive parts.
Various studies are focused on developing glucose biosensors which are also very demanded by the biosensor market, mainly due to diabetes [68][69][70]. Very recent study [71] used CVD graphene without transferring step. Graphene was grown directly on SiO_2, which simplified fabrication process and saved graphene from metal residues which are contaminating graphene and decreasing electrochemical properties. As for other glucose sensors, the graphene was functionalized by glucose oxidase (GOx) and achieved sensitivity was 16.16 µA$mM^{-1}cm^{-2}$ with a LOD 124.19 µM, Fig. 1.16b.

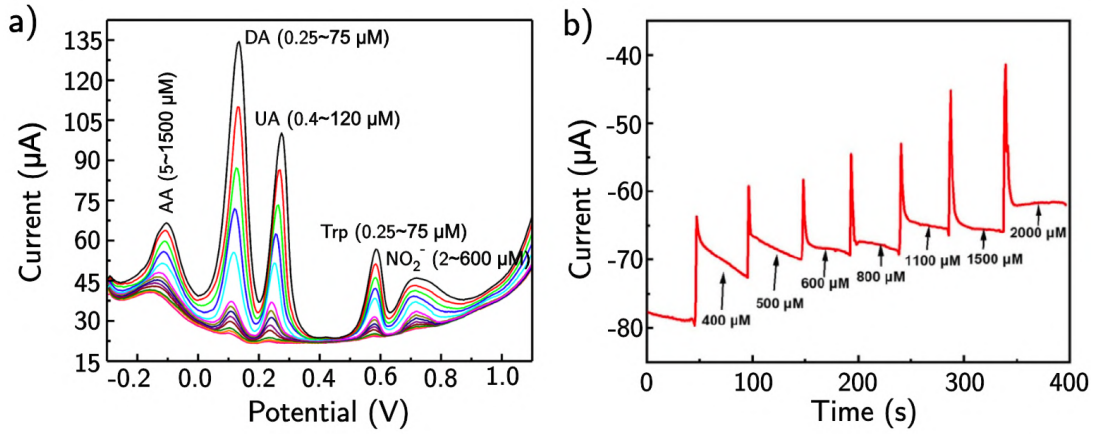

Fig. 1.16: a) DPV curves for Ta/graphene wires in 0.1 M PBS buffer pH 7 for different analyte concentrations. Adapted from [67]. b) Amperometric response with dropwise addition of glucose from 400 µM to 2000 µM. Adapted from [71].

2 Experimental part

The thesis aims to fabricate biosensors suitable for wearable applications monitoring skin wound condition. It can be done with monitoring pH as it is a parameter which is relevant to the skin condition and possible local infections in the wounds. Increasing pH can be a preliminary factor for the bacteria growth [72]. Typical progress of the wound healing is that it starts with slightly alkaline pH ($\sim$ pH 8-9) and as the healing process progresses, the pH goes back to neutral values and finishes the process of successful healing with $\sim$ pH 6 which is typical for healthy skin [73].

2.1 Materials

Biosensor prepared for the thesis has to meet these criteria:

1. **Sensitivity**. The main parameter for material used in the sensor is the highest possible sensitivity to the desired analyte.
2. **Flexibility**. Biosensor should be flexible as it is planned to be applied directly on the skin.
3. **Biocompatibility**. Material is going to be in direct contact with the skin. Thus, it has to be biocompatible.
4. **Conductivity**. The material should have sufficient electrical conductivity so we can read the value from the sensor.
5. **Functionalisation**. The possibility of biosensing directly from the skin is the desired ability for many applications. If the sensor can be functionalised for specific analytes, we can acquire much more information from the skin surface. A proper functionalisation can make the biosensor more robust and can prevent interference from unwanted analytes. For example, we might discover that observing only pH is not sufficient, but we also need to sense bacteria metabolites to identify the infection.
6. **Cost**. Wearable sensors are expected to be periodically changed. Accordingly, the price for the whole sensor is expected to be reasonable so that it can have an important price advantage over the laboratory testing.
7. **Energy efficiency**. This type of sensor is expected to be light-weight, providing sufficient comfort while wearing it. At the same time, the sensor has to be able to measure data for a longer period. Hence, the sensor should be energy efficient as a bulky battery can increase size, weight and overall discomfort of wearing the sensor.

Material which fulfils these criteria is graphene. It has a vast surface area; it is only the surface without the bulk. Thus, it is highly sensitive when the static charge on the surface is changed. At the same time, it is flexible, biocompatible and has required electrical conductivity. The functionalisation of graphene is uncomplicated in the direction of π orbitals thanks to the van der Waals forces. Production costs and scalability of graphene are still probably the biggest issue. Graphene is a relatively new material and its production for industry use is in its beginning. Production costs are still reducing and new promising methods are frequently presented [74][75].
Graphene is only a one atom layer thick material and needs some support to lay on.

Such supportive layer is in the most cases SiO_2. This combination is used in fundamental research because the graphene has the highest electron mobility and can be back gated. However, SiO_2 is not the best choice for our sensors as it is not lightweight and flexible. Therefore, the main measurements were done for graphene on parylene C, which meets all the criteria mentioned above. We also created graphene on SiO_2 samples. Such samples can be interesting for creating sensors on which we put the solution with the analyte (lab-on-chip). Most of the measurements and experimental work were done on the graphene/parylene samples, but we also performed experiments on the graphene/SiO_2 samples for the comparison. Properties of graphene/SiO_2 are much deeply studied in the literature.

2.1.1 Sensor description

The essential and most crucial part of the sensor is graphene. Majority of the experiments was done on graphene without any surface functionalisation. We also prepared a few samples with functionalisation as an extension of this work.
Nevertheless, the thesis aims to describe direct graphene response on various pH. In the future and for additional research, functionalisation can make the sensor more robust, specific, stable, sensitive and mainly, can prevent other analytes interference.
The first type of the samples, graphene on parylene C is described in Fig. 2.1. Graphene on parylene stripes have $2.0\,\mathrm{cm} \times 0.5\,\mathrm{cm}$ and bordered area for applying droplet is $1.0\,\mathrm{cm} \times 0.5\,\mathrm{cm}$. From this information, it is obvious that we are studying macroscopic large-area graphene sheet.
The second type of samples is graphene on SiO_2. The fabrication process of this type of samples allows us to control sample size with higher precision. All samples had $0.5\,\mathrm{cm} \times 0.5\,\mathrm{cm}$ golden pads, which were in three different distances from each other (5, 10 and 15 mm), see Fig. 2.2. The golden pads were prepared at the Central European Institute of Technology (CEITEC). The graphene was transferred between these golden pads and created electrical contact between them. The golden pads were used as a contacting area for wires. The droplet area was bordered by "Freegel" film (GELPAK®), which can be very nicely cut and applied onto the surface. It is a thick hydrophobic silicone-like material. The samples were always connected to an electrical circuit with conductive silver paint.

2.2 Experiments

We used two different experimental setups to measure sensor response to different pH solutions. The first experiment had a straightforward setup and measured resistance dependency on time while we are applying different solutions. Let us call this experiment $R(t)$ experiment. The second experiment was more dedicated using a lock-in amplifier and a liquid top gate to observe doping of graphene. Let us call this second experiment $R(V_g)$.

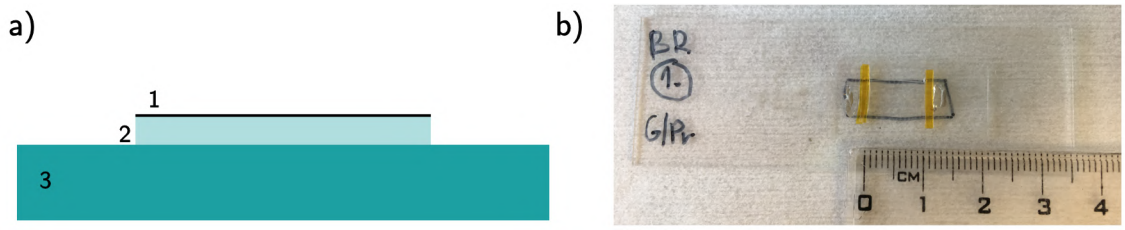

Fig. 2.1: The sample of graphene on parylene. a) Schematic description. (1) is graphene, (2) is parylene C as a supportive layer with a thickness in the order of tens of µm, (3) is a plastic/glass slide used in optical microscopy as the sample bed. Graphene/parylene C was adhered onto the plastic slide by a double-sided scotch tape. The plastic slide is securing graphene and allowing better manipulation. b) Real photo of the sample. The blue lines are eye-guides because all parts are transparent. The yellow lines are Kapton tape which is bordering the area where the solution is applied.

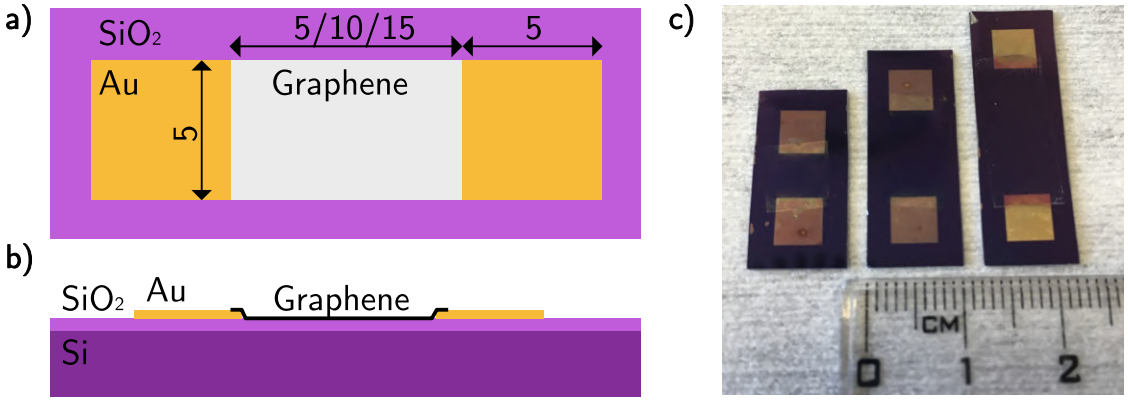

Fig. 2.2: Graphene on SiO_2 sample. Sizes are in mm. Three types of samples were created varying in graphene length; 5, 10 and 15 mm.

2.2.1 Resistance on time dependency

The electrical circuit for this experiment is simple and measures the resistance of the sample. For graphene/parylene C samples, the voltage source and amperemeter are both served from Keithley 6430 connected to PC and controlled by LabVIEW, Fig. 2.3. The source voltage is set to $U = 0.1\,\mathrm{V}$. Resistance was calculated from the current decrease. Graphene/SiO_2 samples measured in Brno had a slightly different setup with current source Keithley 6221 AC/DC Current Source and Keithley 2182 Nanovoltmeter, Fig. 2.4. We used current source with $I = 0.1\,\mathrm{A}$ and $1\,\mathrm{k\Omega}$ resistor in series. The resistance was calculated from a voltage difference read by Keithley 2812 Nanovoltmeter.
The resistance of graphene without applied liquid varies in range 2–30 kΩ. It is crucial to prevent the contact of the droplet with silver paint contacts. We used hydrophobic Kapton tape, and later "Free-gel" film (GELPAK®), for bordering this area and preventing the contact as mentioned in Fig. 2.1b. If the droplet is not in contact with silver paint, the resistance change is caused by the change of graphene

properties in the area where is the droplet applied. The outcome of this result is a description of direct response on different pH that can be easily measured.

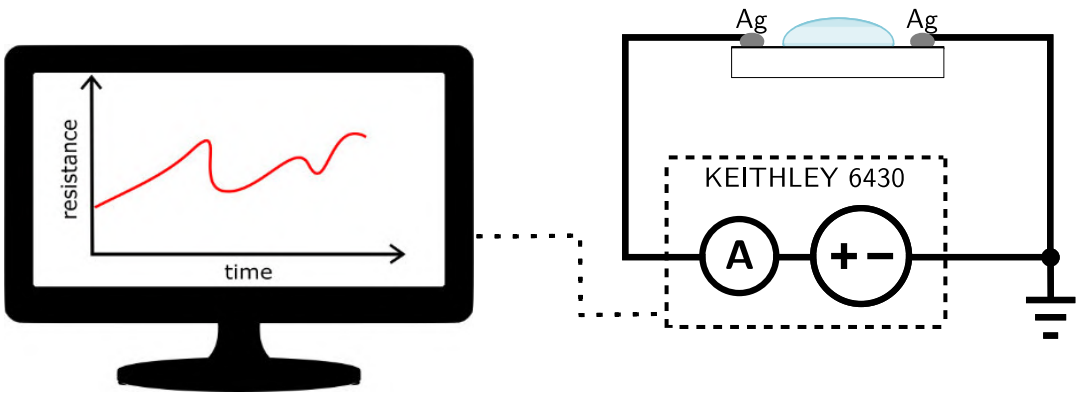

Fig. 2.3: Circuit for the $R(t)$ experiment at Le Centre national de la recherche Scientifique (CNRS) in Grenoble.

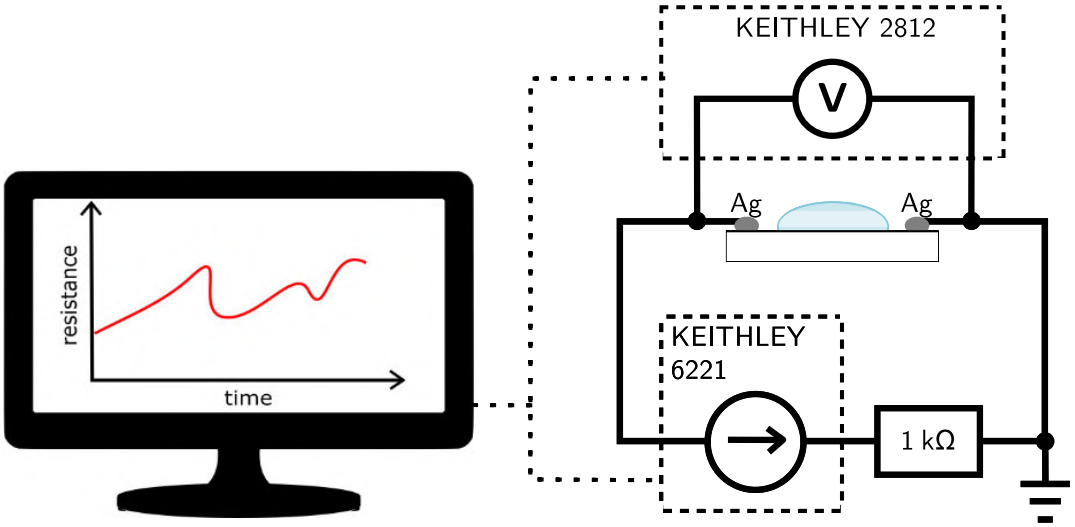

Fig. 2.4: Circuit for the $R(t)$ experiment at Institute of Physical Engineering (IPE) in Brno.

2.2.2 Resistance on gate voltage dependency

The second type of experiment is focused on the electronic characterisation of graphene. We are using the field-effect transistor assembly for this purpose. Graphene is gated via the liquid top gate and we are looking for a change of conductance or resistance, respectively. The point where the value is the lowest, resp. the highest is called the Dirac point. At this point, the number of free charge carriers is the lowest, and it is also the turning point for the type of major charge carriers (from electrons to holes and vice versa).

This experiment is using a more dedicated tool, a lock-in amplifier Stanford Re-

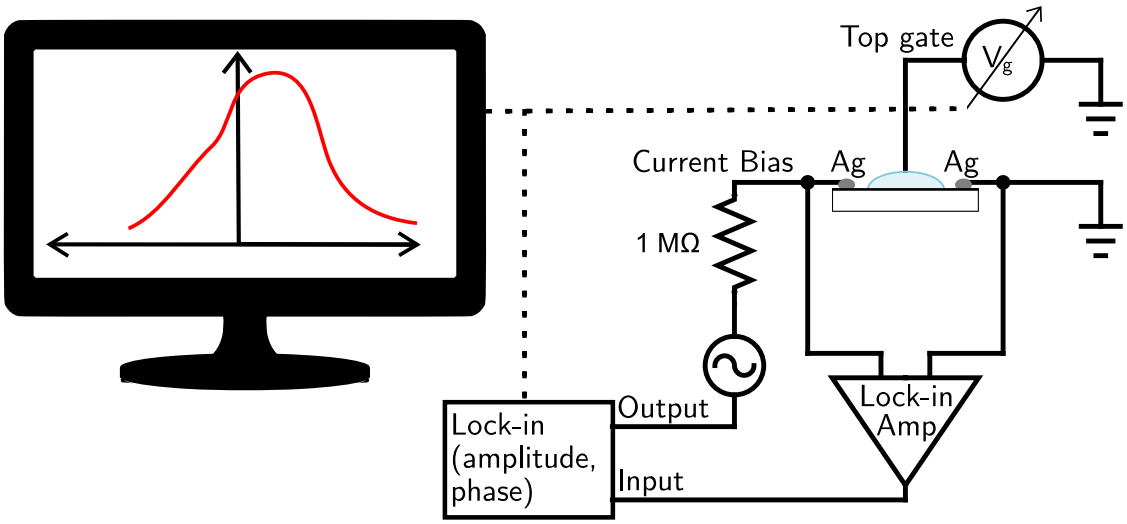

Fig. 2.5: Setup for $R(V_g)$ experiment in Grenoble, France, and illustration of typical outcome processed by PC.

search SR830 which is making measurement more precise even in a noisy environment, Fig. 2.5. The setup in Brno is the same except the resistor 1 MΩ is replaced with 10 MΩ resistor. Lock-in settings were the same for both laboratories (Grenoble and Brno) except the signal frequency. The signal amplitude is 1 V, time constant 100 ms and frequency 10 Hz in Grenoble and 1068 Hz in Brno. It is recommended to measure at lower frequencies with a lock-in amplifier but when we set 10 Hz in Brno, the data were too noisy. The problem might have been that the setup in Brno had a lot of electrical devices and vacuum pumps running in the same room. Both electrical and mechanical noise could have disturbed the measurement. Thus, we tried various frequencies and the value 1068 Hz gave us convenient results.

The most important part of $R(V_g)$ experiment is the liquid top gate. The gating needle penetrates droplet and at the same time does not touch the graphene surface, Fig. 2.6b. The voltage ranges from -1 V to 1 V and is applied to the needle; the change of graphene resistance is observed. When graphene is on SiO_2 the back gate is more common than top liquid gate, Fig. 2.6a. We also did an experiment with a back gate for comparison. However, back gated graphene is not an ideal solution for our device because of a few reasons.

First, the capacitance of the back gate is much lower and we need to apply much higher range of voltage, Fig. 2.6c. Common gap width d for the back gate is $\sim$ 300 nm. This value is much higher than the gap of the EDL layer in order of only a few nanometers, as explained in the theoretical part. For illustration, the typical range for back gate voltage is ca. $\pm$70 V, which is dramatically higher than the top liquid gate voltage ca. $\pm$1 V. At the same time, we are trying to create a light-weight, energy-efficient device. Therefore, the lower applied voltage is desirable. The used experimental setups are shown in Fig. 2.7.

The outcome of this measurement is $R(V_g)$ curve describing the doping of graphene. The Dirac point in real graphene samples is only rarely exactly at 0 V as it should

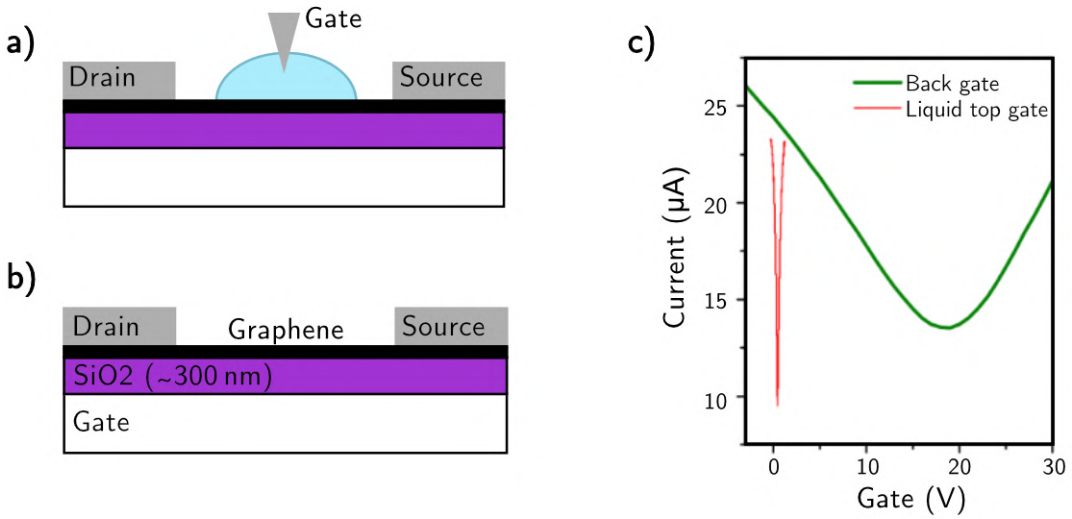

Fig. 2.6: Two possible gating modifications for observing $R(V_g)$ dependency. a) back gate, b) liquid top gate and c) comparison of field effects.

be for pristine graphene without any doping.
Graphene used in this thesis went through the fabrication process and its supportive layer is parylene C or SiO_2. All of this caused doping of graphene and shifting the Dirac point. This is a characteristic parameter for each device and is changing through the device lifetime based on the environment, adsorbates, mechanical processes, etc. For example, application of various pH with different H^+ and OH^- ions ratio is affecting the surface static charge and electrochemically doping graphene and shifting the Dirac point.
Each pH should shift $R(V_g)$ curve as the overall doping of graphene changes. Another meaningful parameter we can read from the curve is the mobility of charge carriers. The steeper the slope of the curve is, the higher mobility carriers have. Parylene C is wrinkled material with defects and average carrier mobility of graphene on parylene is lower than on SiO_2.

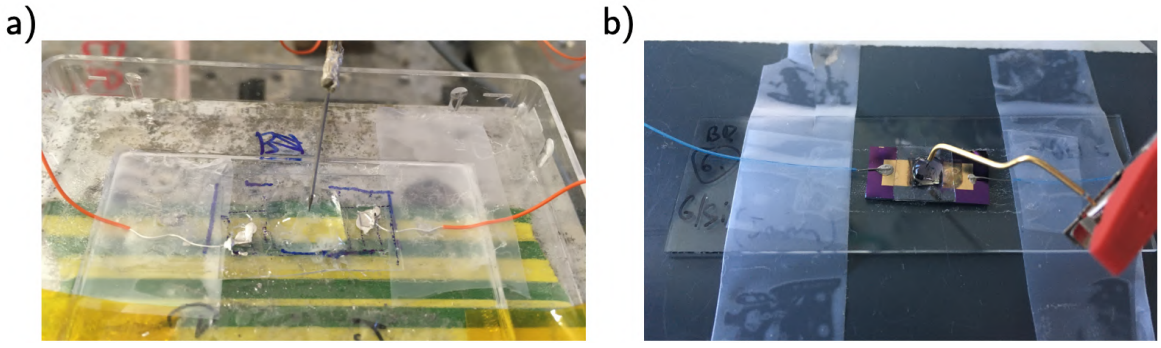

Fig. 2.7: Device setup for measurement with liquid top gate. a) Setup at CNRS, Grenoble in France. b) Setup at IPE in Brno.

2.3 Resolved challenges

We discovered some challenges during the initial experiments. Detailed solutions are mentioned in this section.
The first challenge was to maintain easier manipulation with graphene on polymer as it is extraordinarily light and crunching material. We used double-sided scotch tape to attach the graphene on a polymer or SiO_2 on a plastic plane. An important parameter was the sample size, and mainly the size of the area where the electrolyte is applied because it is sensing area of the sensor. Therefore, we bordered the area by hydrophobic Kapton tape, Fig. 2.1b, and later by "Free-gel" film (GELPAK®). Stripes of graphene/parylene had size 2.0 cm × 0.5 cm with 1.0 cm × 0.5 cm sensing area. The graphene/SiO_2 samples varied in size and the sensing area - $(0.5 \times 0.5;\ 1.0 \times 0.5;\ 1.5 \times 0.5)$ cm^2. The liquid (150 µL) was pipetted into this area and created a bulky drop which was easily penetrable by the gating needle.
The first set of experiments was focused on understanding electrolyte, measurement

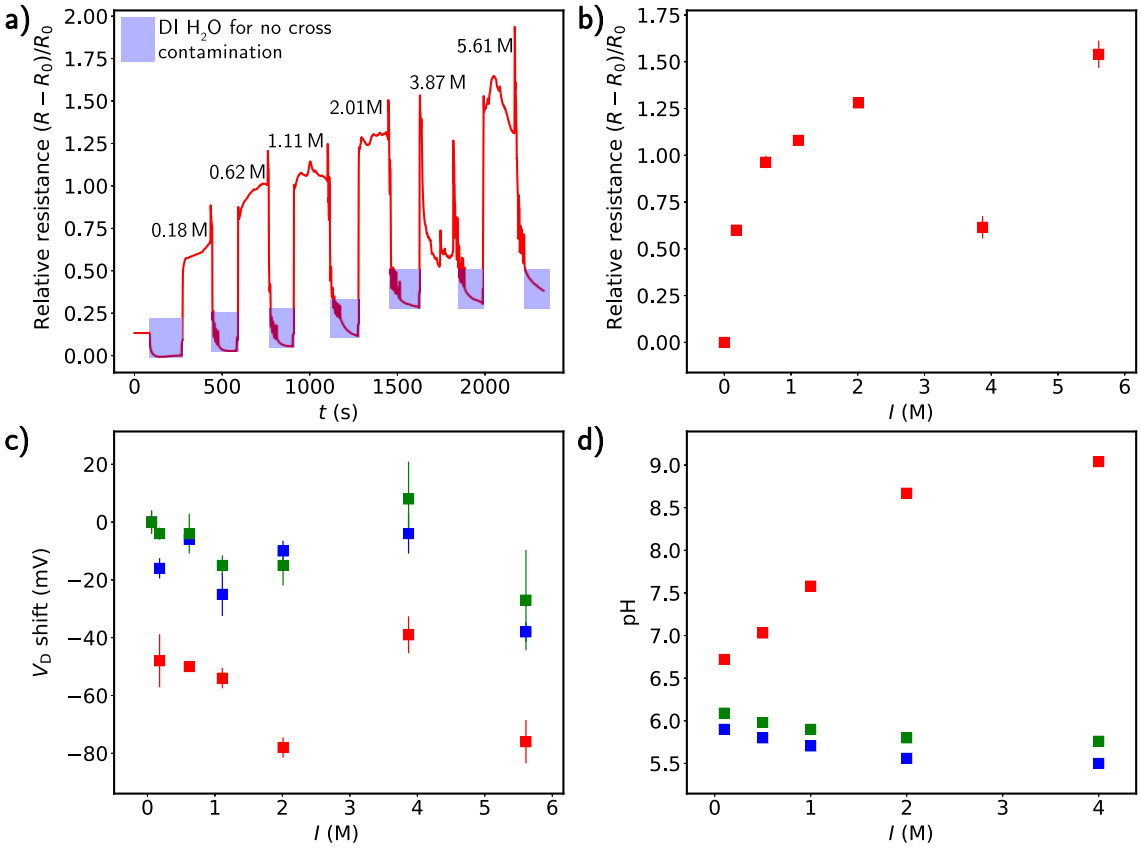

Fig. 2.8: Set of experiments for different ionic strength. a) R(t) measurement as a function of ionic strength in range from 0.18 M to 5.61 M. b) Results from a) recalculated relative to DI water, which can be seen around 50 s. Value for 3.87 M is not with a perfect agreement with other points as we can see from both plots a and b. c) The shift of Dirac points V_D for three different samples (red, blue, green). d) Change in pH measured by electrode pH meter for laboratory (blue and green) and kitchen (red) NaCl.

errors and ionic strength. Important results (Fig. 2.8a,b) are showing us that buffers with constant pH 6 but varying ionic strength are significantly changing graphene resistance. The sample was rinsed with deionized (DI) water between each change of solution to prevent cross-contamination. Ionic strength was changed by the addition of pure NaCl and then recalculated. Due to these results, we also expected the Dirac point shift which had not been confirmed. We see measurements for three samples in Fig. 2.8c. The outcome is a slight move towards the negative gate voltage. The change is slight and the points are not following any stable trend and are rather fluctuating around the initial value which is pure pH 6 buffer without any additional NaCl.
Solution's pH was measured with CyberScan pH5000 manufactured by Eutech Instruments, see Fig. 2.9. This pH meter is using an electrode with a bulb from special glass (membrane) which is penetrable for ions. When the solutions have different acidity, ion exchange is encountered. Such exchange causes a potential change in the range of tens to hundreds of mV.
Measurement is accurate for solutions with lower concentration as higher concentrations can interfere with the measurement. We verified this by experiment that can be seen in Fig. 2.8d, where we measured DI water and changed only the salt concentration. We used two different types of NaCl for this experiment; the first is ultrapure NaCl for laboratory purposes (blue and green), the second is NaCl (red) that is used in the kitchen and can be bought in any shop. The error went up to 0.3 pH points at 4 M concentration for ultrapure NaCl. It is not so surprising that higher concentrations (more ions) are causing measurement errors. Nevertheless, this was not concerning us as we are using low concentration buffers with ionic strength 150 mM. A few initial experiments were done with solutions with the addition of classical kitchen NaCl from the institute canteen. The results were not very persistent and not reproducible. In Fig. 2.8d we saw a significant change of pH (red) when compared to pure laboratory salt. Once again, it is not very surprising as there are some additions to the kitchen salt. We confirmed that kitchen NaCl in unacceptable and we used only pure laboratory NaCl for all the other experiments.
We aimed at measuring different pH. Initially, we started experiments with bought buffers (pH 6, 7 and 8). Soon, we realised how important is ionic strength in the EDL and behaviour of electrolytes in general. Based on the accessible information from the manufacturer bought buffers had each different ionic strength. Therefore, we decided to create our buffers with controlled ionic strength. The buffer production is mentioned in the upcoming section.

2.4 Buffer preparation

Because of the mentioned reasons, we created our buffers. First of all, buffers are solutions which resist pH changes when acids or bases are added to it [79]. Each salt which is used as a fundamental part of the buffer has a different value of pK_a. pK_a is a negative logarithm of dissociation constant $\mathrm{p}K_\mathrm{a} = -\log K_\mathrm{a}$. Acid dissociation constant K_a is describing the strength of the acid in solution. The buffers do not have linear pH dependency on the added volume of base or acid, Fig. 2.10b. The values around $\mathrm{p}K_\mathrm{a}$ points are more stable. Thus, it is recommended to create buffers with

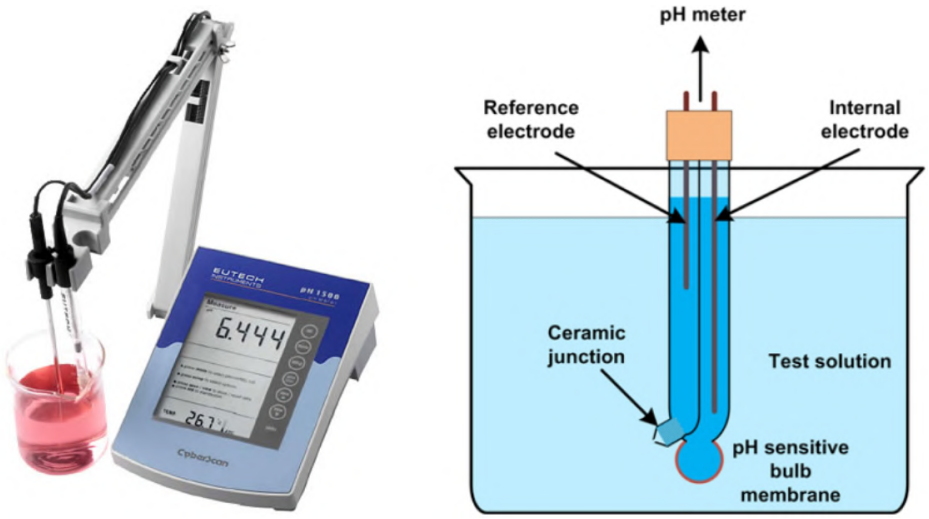

Fig. 2.9: Left: Image of the pH meter used for the measurements [76]. Right: Basic overview of the electrode. Reference Ag/AgCl electrode is in KCl solution. Internal electrode is filled with HCl [77].

$\mathrm{pH} = \pm 1 \mathrm{p}K_\mathrm{a}$. Buffers usefulness is visible in Fig. 2.10a where is displayed buffering capability of water. Water is also a buffer but a terrible one.

We prepared two different buffers - phosphate and HEPES.

HEPES (4-(2-hydroxyethyl)-1-piperazineethanesulfonic acid) is a versatile buffer used in biological research for cell cultures. It has recommended pH range from pH 6.8 to pH 8.2. Notable is that HEPES is not cytotoxic to monolayer cultures and is evaluated as a tissue culture buffer [78].

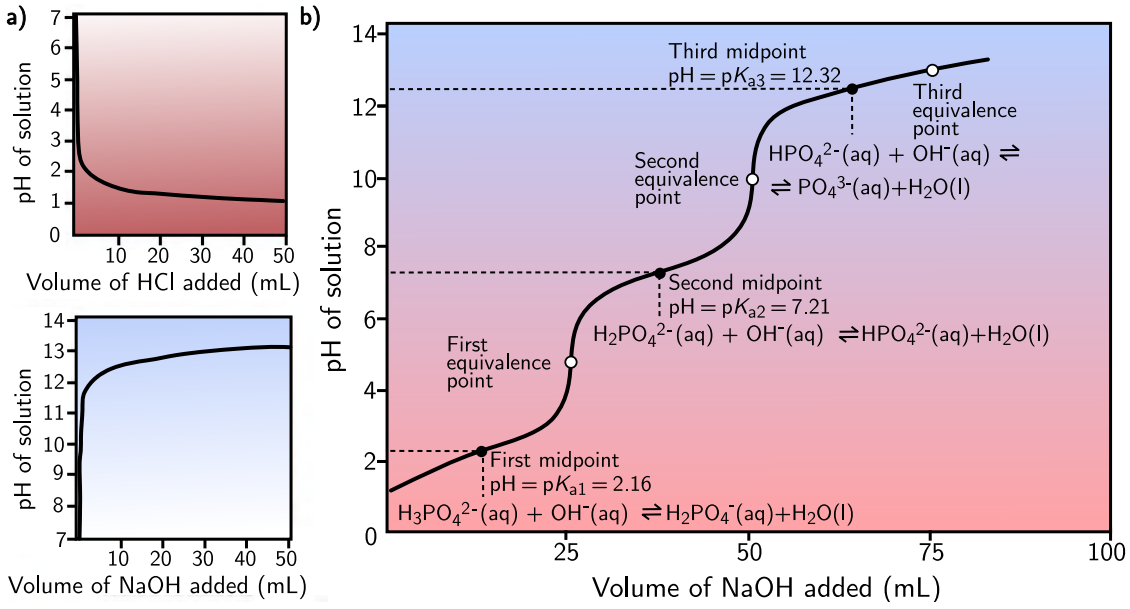

Fig. 2.10: a) Buffering capabilities of water. b) Titration curve of phosphate buffer [80].

Phosphoric acid in phosphate buffer is triprotic acid and undergoes three dissociations ⇒ three different pK_a points (pK_{a1} = 2.12, pK_{a2} = 7.21, pK_{a3} = 12.44), see Fig. 2.10b. The buffer was created from Na_2HPO_4 salt and we had been using this buffer more frequently as it was prepared first and we are going to describe its preparation below.
Ionic strength of the final solution was set to $I = 150\,\text{mM}$, which is very similar to physiological saline solution used in medicine ($I = 154\,\text{mM}$). Molar concentration of buffer was $c = 50\,\text{mM}$ and the desired ionic strength is provided by addition of NaCl. Needed volume of NaCl is always different, because ionic strength of 50 mM Na_2HPO_4 is pH dependent as we can see from Fig. 2.10b as we are changing ratio of $H_2PO_4^-$ and HPO_4^{2-}, and the ionic strength is dependent on the ion charge number z as z_i^2.
Three buffers were created around phosphate pK_2 point 7.21. Buffers with pH 6.2, 7.2 and 8.2 were created by titrating solution with 1 M NaOH. Same process was repeated for HEPES buffer and buffers with pH 6.7, 7.7 and 8.7 were created.

2.5 Results

Results can be divided into two parts. Majority of experiments were performed at CNRS laboratories in Grenoble, France. At CNRS facilities, we used graphene on parylene produced by company GrapHeal. Rest of the experiments with graphene on SiO_2 was performed at the IPE at Brno University of Technology.

2.5.1 Graphene on parylene C

The prime goal of these experiments is to describe graphene on parylene devices (Fig. 2.1) and its behaviour as a function of pH.

$R(V_g)$ experiment

Six samples from three different graphene sheets were successfully measured and processed. Typical outcome of $R(V_g)$ results can be seen in Fig. 2.11.

Overall view of all measurements is displayed in Fig. 2.12. Dirac points are shifted for both buffers into negative values with increasing pH. We conducted ten successful measurements for phosphate buffers (red) and three for HEPES buffers (blue). Each point is average from three R(V_g) curves with relevant error bars. The measured samples were prepared from three different graphene/parylene C sheets varying in quality, resistance and also the age. We can see (Fig. 2.12b) that all the samples are p-doped except for the two samples. These two samples have the highest resistance (15 kΩ–17 kΩ) and the graphene is the oldest.

We statistically processed measured data with 95 % confidence interval (used in the whole thesis) and conclude that the Dirac point shift is $(23 \pm 9)\,\text{mV/pH}$ for phosphate buffer and $(32 \pm 16)\,\text{mV/pH}$ for HEPES buffer. The error for HEPES buffer is higher mainly due to the lower number of measurements.

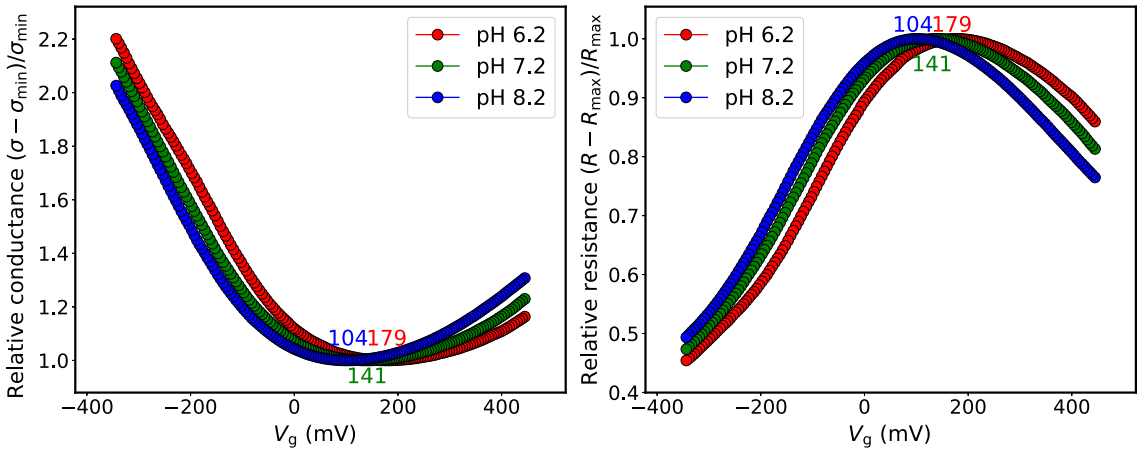

Fig. 2.11: Typical outcome for $R(V_g)$ measurements. The number at extremes are Dirac point values in mV. Left: Plot with conductance, where we can see the lowest conductance in Dirac point. Right: The same plot shown with relative resistance which is easier to imagine and is commonly used.

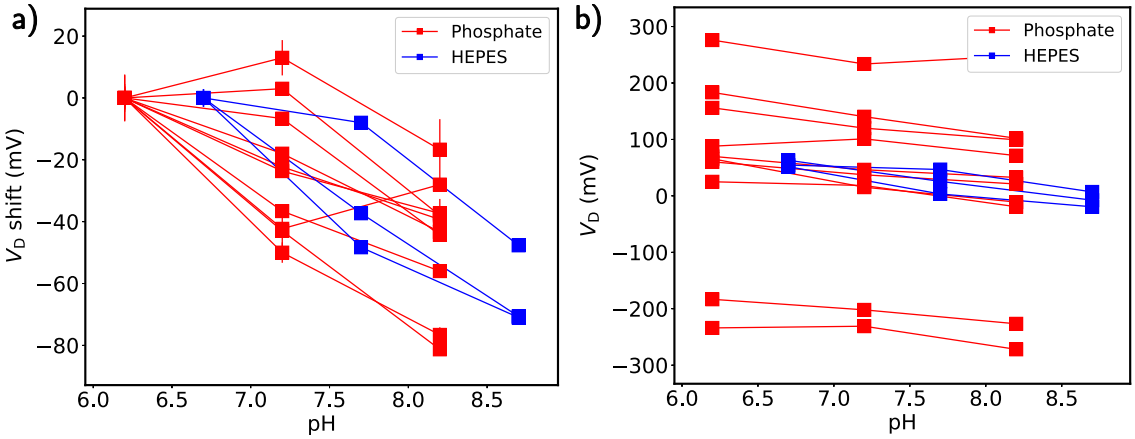

Fig. 2.12: All results for $R(V_g)$ experiment with graphene/parylene C. a) Values are taken relative to the value for the lowest pH; 6.2 for phosphate buffers and 6.7 for HEPES buffers. b) Absolute V_D values. We can see widespread initial values caused by doping.

$R(t)$ experiment

Results of this experiment are more critical for future applications. Measuring device's resistance is straightforward and less demanding.
Firstly, we let sample 50 s in ambient conditions, see Fig. 2.13. After that, we applied DI water for 100 s, and this value was used as R_0. Thanks to this, we were able to extract relative resistance change and compare samples because they varied a lot in the absolute values of resistance (2 kΩ–30 kΩ). Typical for all the measurements is saturation time. The resistance is saturating until more stable R value. We changed the pH solution every 100 s, so the data can be easily processed and compared.
We cleaned the sample between each change of solution by DI water (Fig. 2.13 blue

areas). We empirically discovered that five rinsings with DI water get the resistance near R_0 and more rinsings were not causing any additional change. We used the pipette to rinse the sample with DI water. We can see in Fig. 2.13 a significant difference between each pH point. One of the essential characteristics of the sensor is the reversibility of measurements, which is clearly shown in Fig. 2.13.

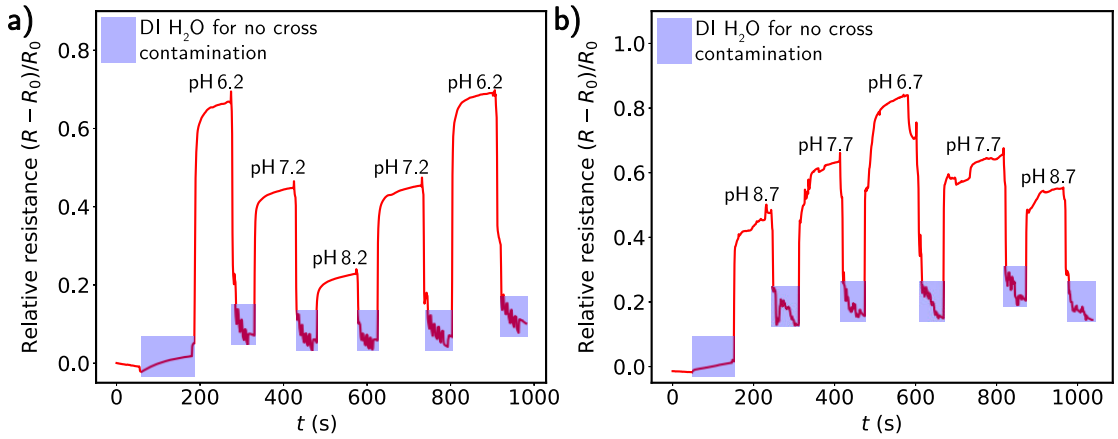

Fig. 2.13: $R(t)$ experiment results for graphene/parylene C. a) Reversibility of results for phosphate buffers. b) Reversibility of results for HEPES buffer.

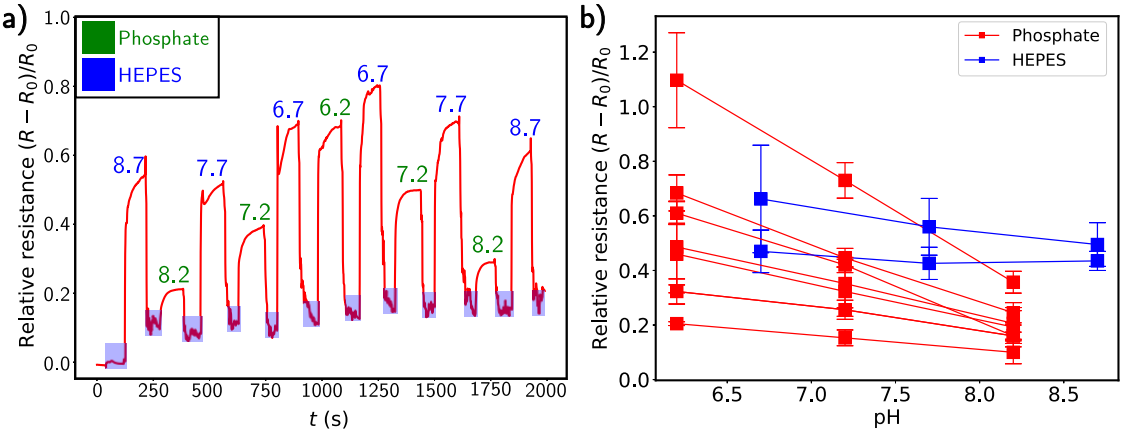

Fig. 2.14: a) Measurement in one sequence for both buffers on one graphene/parylene C sample. Numbers are pH values. Blue areas are rinsing with DI water. b) All $R(t)$ measurements for graphene/parylene C samples. Measurements were done for both buffers (phosphate, HEPES).

More challenging measurement with both buffers is in Fig. 2.14a. The reversibility is demonstrated again for phosphate buffer. The results for HEPES buffer are not so conclusive. We sequentially applied solutions from the highest pH 8.7 until the lowest pH 6.2. We would expect a sequential increase/decrease in sample resistance, which we do not see. Therefore, the possibility of other influencers than pH should be considered. Based on the data, it seems like buffer molecules might

Tab. 2.1: Relative change of resistance for phosphate buffers.

pH ()	6.2	7.2	8.2
$\frac{R-R_0}{R_0} \cdot 100$ (%)	55 ± 9	38 ± 5	22 ± 4

also interact with graphene. For example, HEPES pH 8.7 has much higher R than phosphate pH 8.2.

We performed a sufficient amount of measurements for phosphate buffers as can be seen in Tab. 2.1. The highest resistance change is for the lowest pH 6.2. The highest relative resistance change is (18 ± 8) %/pH. Both buffers have the highest resistance for the lowest pH values 6.2 and 6.7. All graphene/parylene $R(t)$ measurements are in Fig. 2.14b. Final summarization of all the samples and both measurements is in Fig. 2.15.

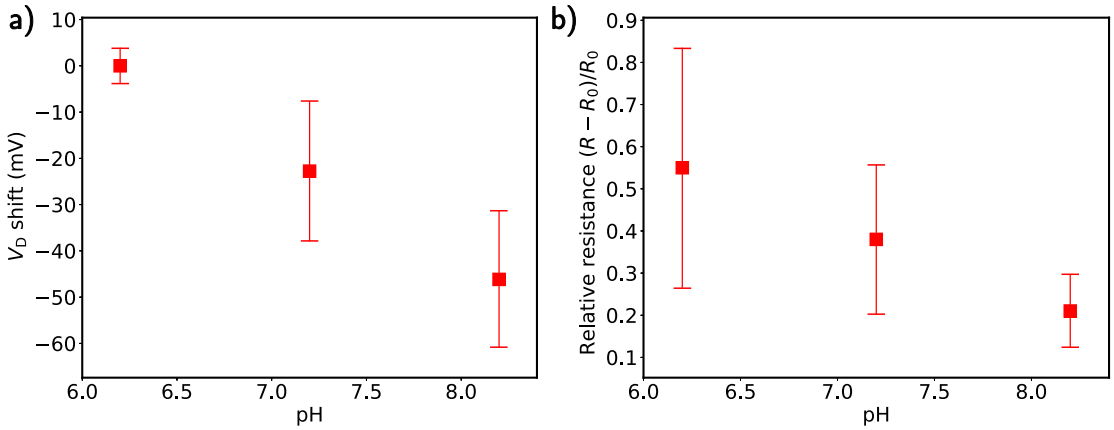

Fig. 2.15: Summary of both $R(t)$ and $R(V_g)$ measurements for phosphate buffers. Results for HEPES do not have sufficient statistic strength. a) Results of $R(V_g)$ experiment for 10 phosphate buffer measurements. b) Results of $R(t)$ experiment for 7 phophate buffer measurements.

Polyaniline functionalisation

We tried to functionalise graphene on parylene C by the method used in the article [81]. They developed low-cost pH sensors from carbon electrodes coated with proton-selective polymer polyaniline (PANI). The main principle is protonation and deprotonation of nitrogen atoms in the polymer chains of PANI. The polymer doped with H^+ ions is called emeraldine salt (ES) and has a slightly green colour. On the other hand, when the H^+ ions are captured, the PANI is neutralised forming blue emeraldine base (EB), and the surface charge and potential is decreased.
The first sample coated with PANI was prepared by drop-casting as described in the article. After that, the dry sample was doped by HCl for 5 hours in the vacuum chamber. We tried to measure $R(V_g)$ curves, but we were not successful. The typical $R(V_g)$ curves were not established as there was no gating effect. The most obvious

explanation would be the high thickness of PANI coating, which prevents graphene from being affected by the gate electric field. After this observation, we created two more samples coated by spin-coating. One sample was spin-coated for 20 s with 500 rpm and the second sample with 6000 rpm.

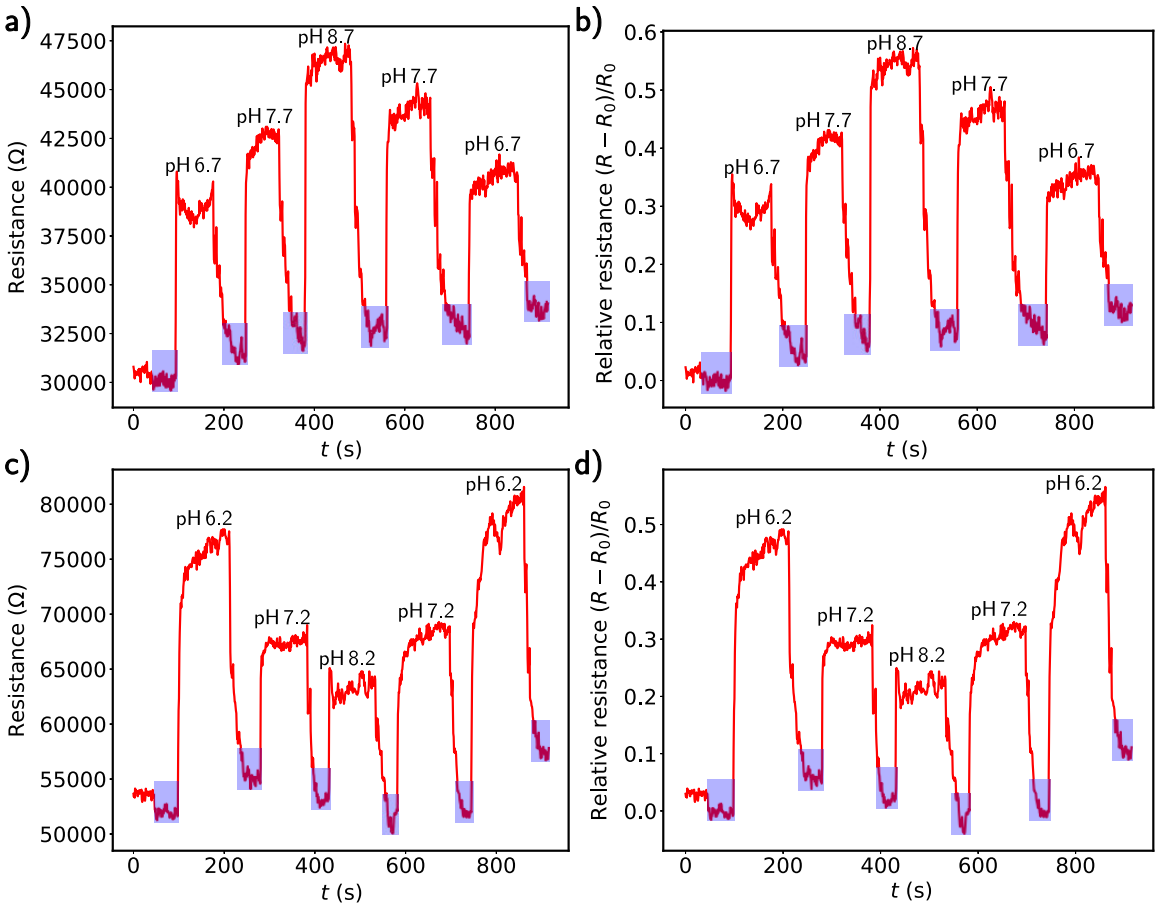

Fig. 2.16: $R(t)$ measurement of graphene/parylene C sample with 6000 rpm spin-coated PANI, which was doped by HCl. a,c) Absolute values for HEPES, resp. phosphate buffers. b,d) Relative values of the same measurements.

These two samples were also doped with HCl and measured by both experiments. The $R(V_g)$ curves were not very convincing. It seemed like even thinner PANI coatings are profoundly affecting gate field effect. We tried to measure the thickness of the PANI coating for this purpose. We used Dektak Profilometer and Atomic Force Microscopy (AFM), but none of these methods was successful. The layer of PANI on parylene is soft and probably not measurable by these methods.
At the end, the sample with 6000 rpm spin-coating was the only measurable sample with consistent $R(t)$ results, Fig. 2.16. We can see in Fig. 2.16a,c the absolute values and that the sample resistance is considerably higher than for samples without coating. The data are noisy for both measurements compared to graphene with functionalisation. Making PANI coating even thinner can properly functionalise graphene without shielding gate field effect. The promising candidate for such test

Tab. 2.2: $R(t)$ measurement experiment for graphene/parylene C with 6000 rpm spin-coated PANI.

	pH ()	6.2	7.2	8.2
$\frac{R-R_0}{R_0} \cdot 100$ (%)	**Phosphate**	46 ± 5	35 ± 3	33 ± 7
	pH ()	6.7	7.7	8.7
$\frac{R-R_0}{R_0} \cdot 100$ (%)	**HEPES**	41 ± 3	45 ± 3	47 ± 3

is graphene/SiO_2 which is smoother and its spin-coating can lead to thinner film than in case of graphene/parylene.

2.5.2 Graphene on SiO_2

We chose graphene on SiO_2 as the material for the second set of samples, Fig. 2.2. These samples are mainly for comparison with graphene/parylene C. We can also apply back gate voltage using the Si layer, Fig. 2.17. All the measurements were done using phosphate buffers because we did not have access to HEPES buffers anymore. The CVD graphene purchased from Graphanea was spin-coated with PMMA and the copper was etched in ferric chloride $FeCl_3$. The graphene on PMMA was fished with SiO_2/Si wafer. The graphene was let to dry and after that, annealed on a hot plate. PMMA layer was removed using acetone.

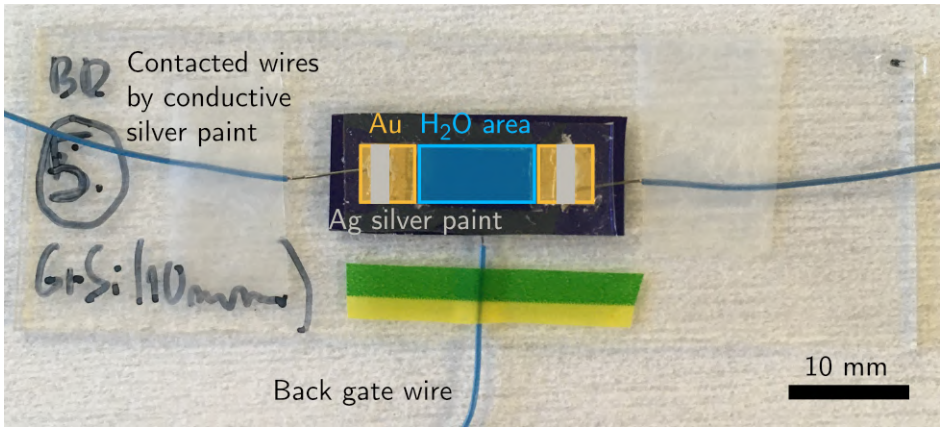

Fig. 2.17: Graphene/SiO_2 sample contacted by the conductive silver paint (silver) to the 5 mm × 5 mm golden pads (yellow). Droplet area (blue) is bordered by "Free-gel" film (GELPAK®). It is possible to apply back gating with the wire contacted to Si layer by the conductive silver paint.

Challenges

Four longest samples were (15 mm) all without continuous graphene layer, Fig. 2.18. The golden pads are in the image sides. Shadow-like squares in the image are the artefact of image stitching. The graphene was cracked on the whole sample, Fig. 2.18b. This problem did not happen for any other sample size. We could

not find any obvious explanation except that the graphene is too specious and was destroyed in the transfer process or the PMMA layer did not hold it properly.

The other samples (5 mm and 10 mm long graphene) had promising electrical prop-

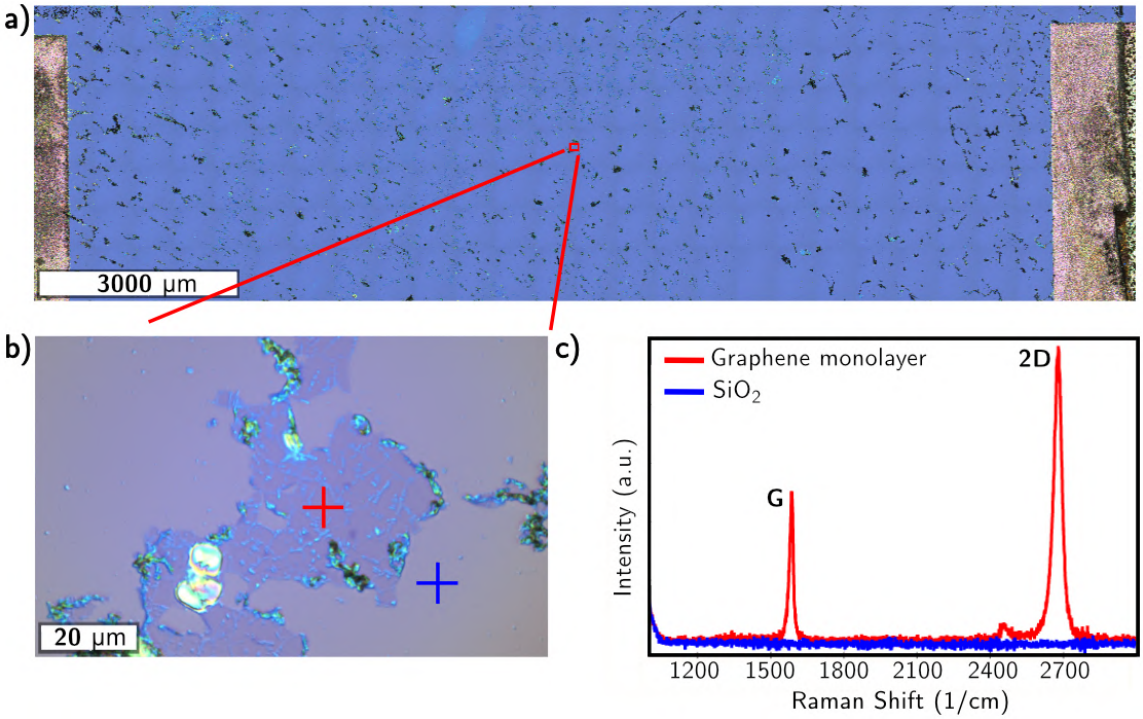

Fig. 2.18: One of the 15 mm long graphene/SiO_2 samples under Raman spectroscopy. b) Detail from the image a). c) Raman spectra from selected points in b) (red, blue).

erties ($R < 15\,k\Omega$) and continuous graphene layer. However, for each sample, the resistance was increasing during the measurements. At a certain moment, the electrical contact was lost and we were not able to measure the sample anymore. At first, we suspected the back gate voltage (± 70 V), which is many times higher than the liquid top gate voltage (± 1 V).

It can be a serious problem if in the SiO_2 (285 nm thick) are holes and defects. In such cases, the electrical current from Si layer can flow through the hole and consequently damage the graphene layer. However, after some additional experiments without applying back gate voltage, the graphene cracking was still evident.

It was the main reason why we decided to investigate the sample by Raman spectroscopy. The first leading point is that the graphene is still continuous near borders of the droplet area. This change is highlighted in Fig. 2.19a with a white dashed line. The area between the dashed line and "Free-gel" film (GELPAK®) is a continuous graphene layer without any significant cracks. Detail of this cross-section is shown in Fig. 2.19b with corresponding Raman spectra. The border between damaged and continuous graphene is clearly visible. The continuous graphene sheet also has imperfections but not in the scope endangering overall electrical conductivity of graphene. Graphene cracking can be caused by these factors: the droplet itself, the measurement (high electrical current, voltage) or the combination of both.

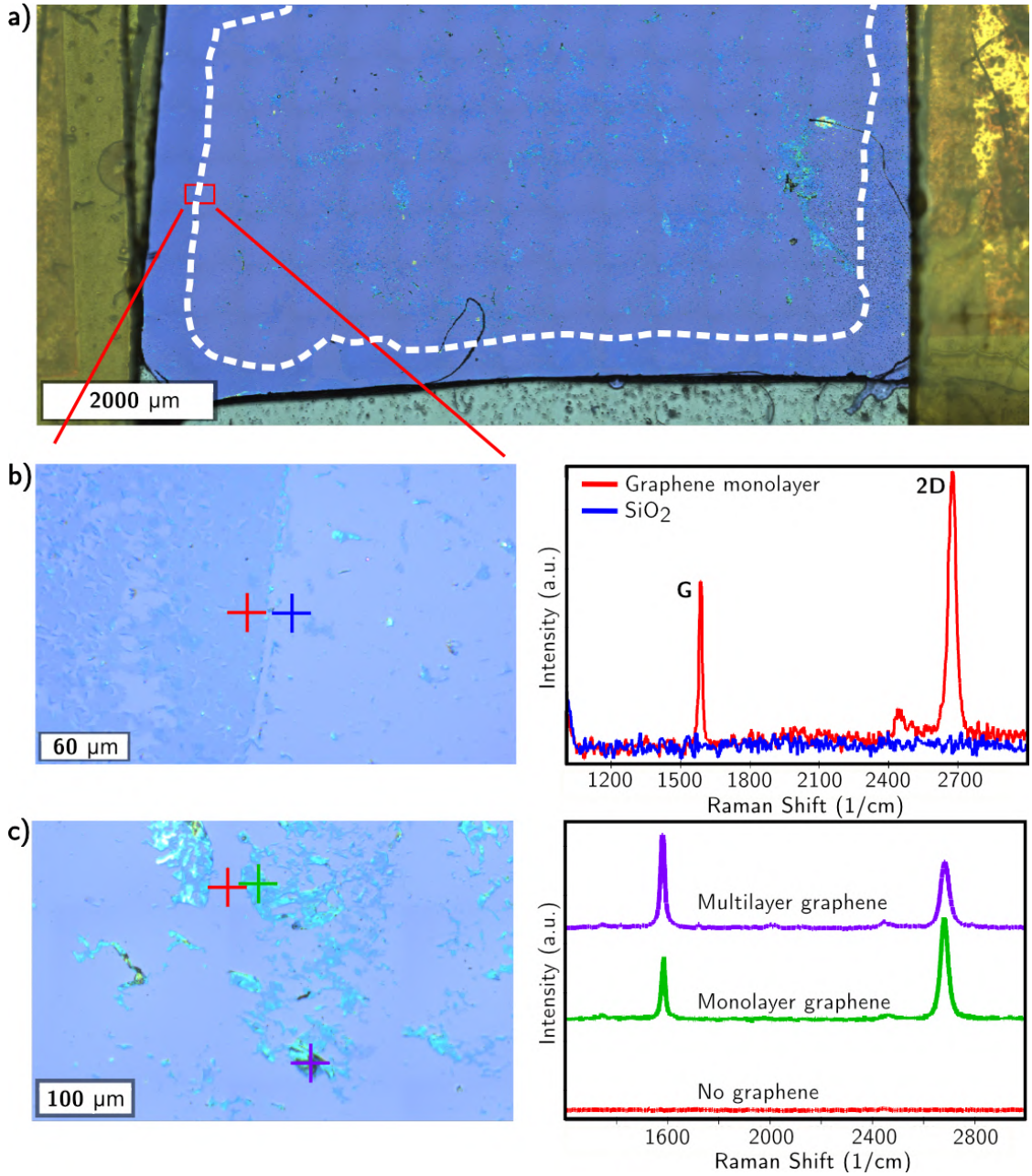

Fig. 2.19: Graphene/SiO_2 sample with 10 mm graphene under Raman spectroscopy. The yellow part in a) is Kapton tape on "Free-gel" film (GELPAK®). White dashed line highlights the border between continuous and cracked graphene. b) Detail from the image a) with two points and their Raman spectra. c) Raman spectra from the middle of the sample with various types of surface.

The next step was to control graphene condition during the measurement. For this purpose, we took a picture of the sample before and after the measurement, Fig. 2.20. The initial resistance of the sample was $R = 9.4\,\mathrm{k\Omega}$. The electrical contact was lost after one R(t) measurement and the condition of graphene had rapidly worsened, Fig. 2.20b.

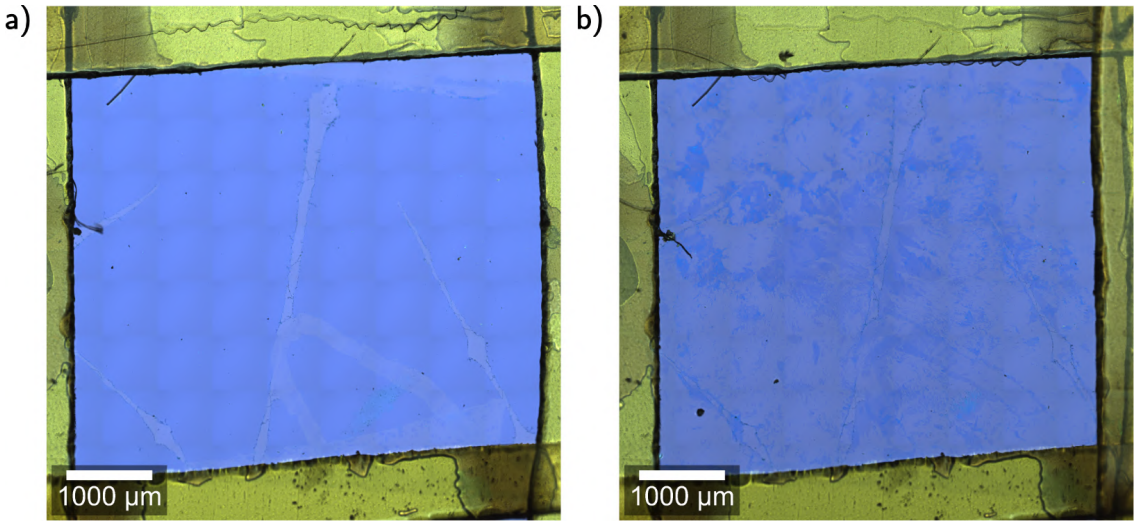

Fig. 2.20: 5 mm long graphene on SiO_2. Shadow-like squares in the image are the artefact of image stitching. a) Before measurements. b) After measurements.

Based on the previous results, we decided to study only water and graphene/SiO_2 interaction. The small DI water droplet was pipetted on the graphene and observed in the optical microscope. The droplet was applied and left to evaporate. The sample was not contacted and it was only pure graphene on SiO_2 without any additional components such as wires, GELPAK®or Kapton tape. The water evaporation took around 10 minutes. We can see the outcome in Fig. 2.21. The initial droplet spread quickly (expanded droplet area) over the surface. Fast droplet spread shows us its hydrophilicity. One of the most compelling areas is the border between the initial and expanded droplet area. We can see noticeable cracking in the direction of water spreading. If we consider capillary pressure which is high since the droplet spread quickly on the surface, the pressure might be high enough to tear the graphene while spreading on the surface. It also makes sense that the damage is the highest at the border between the initial and expanded droplet. The droplet holds the initial position and the biggest force is pulling it in the moment of initial spreading. We can also see many small residues in the drying centre where the water brought it. The problem can also be the wet transfer of graphene which could let some water between graphene and SiO_2. Based on the study published by Rafiee et al. [82], the graphene is wetting transparent in the most cases (silicon, copper, gold) and, therefore, hydrophilic on SiO_2 [83][84]. Both findings support our explanation. Moreover, if some water stayed between graphene and SiO_2, the water molecules under graphene may try to hold together with water molecules on the surface.

To prevent this issue, we annealed the samples in a vacuum chamber (1 h annealing at temperature $t = 200\,°C - 250\,°C$, and pressure $p = 1\,Pa$). After the annealing, we repeated the experiment with the droplet evaporation. This time, the graphene stayed intact. We conclude that previous low adhesion of graphene on SiO_2 was the main factor responsible for the sample destruction. Quickness and magnitude of destruction can be seen in Fig. 2.22. The graphene quality is often classified by carrier mobility μ, which rapidly decreased in our case.

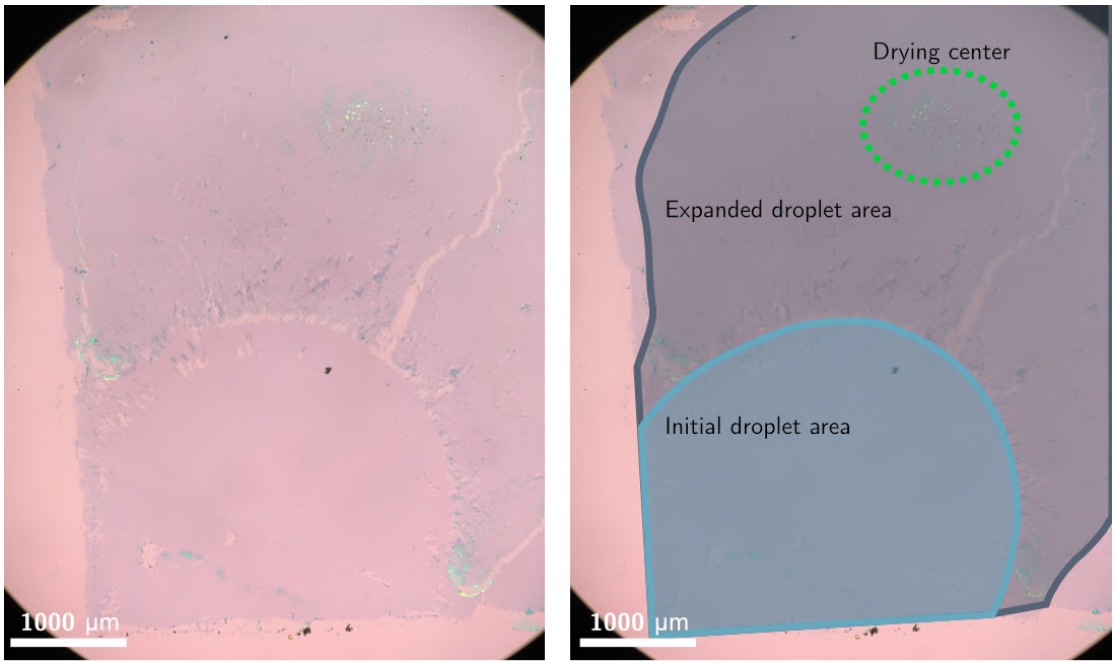

Fig. 2.21: Observation of water on the graphene/SiO_2 sample. Initial droplet area is a place where we pipetted DI water. The droplet spread on the surface in a few seconds (expanded droplet area). The droplet was slowly evaporating and terminated its drying at the drying centre area.

From $\mu_{\max} = (5280 \pm 70)\,\mathrm{cm^2V^{-1}s^{-1}}$ to $\mu_{\min} = (1540 \pm 10)\,\mathrm{cm^2V^{-1}s^{-1}}$. Mobility fit was taken from electron region by the least squares fitting method and function from [85]. The mobility is mainly affected by impurities and defects [86], and cracks in graphene (Figs. 2.20, 2.21) can be certainly responsible for such phenomena.

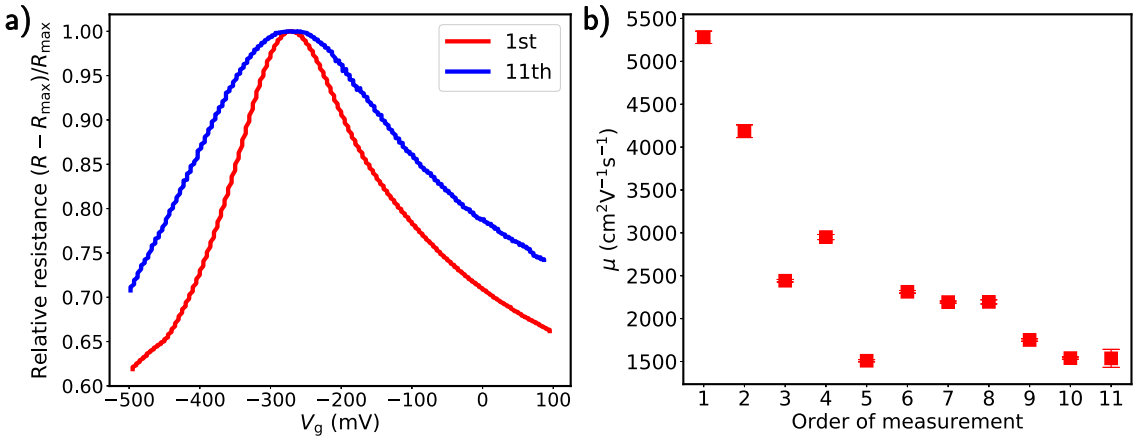

Fig. 2.22: Eleven $R(V_g)$ sequential measurements of graphene/SiO_2 sample. a) Change of $R(V_g)$ curve shown on 1st (red) and 11th (blue) measurement. Blue curve was shifted $-83\,\mathrm{mV}$ for better illustration and visual comparison. This $-83\,\mathrm{mV}$ V_D shift is not necessarily caused by the sample degradation because the 11th measurement is for different pH. b) Carrier mobility μ obtained from electron region.

$R(V_g)$ experiment

Due to the challenges mentioned above, obtaining relevant data was more complicated than for graphene/parylene samples. The main problem was the reproduction of the results because the samples endured only a few measurements. This is the case even for samples after annealing, which were more durable, but considerable devaluation was still visible.

We see in Fig. 2.23 that the visual trend is not so convincing as the graphene/-

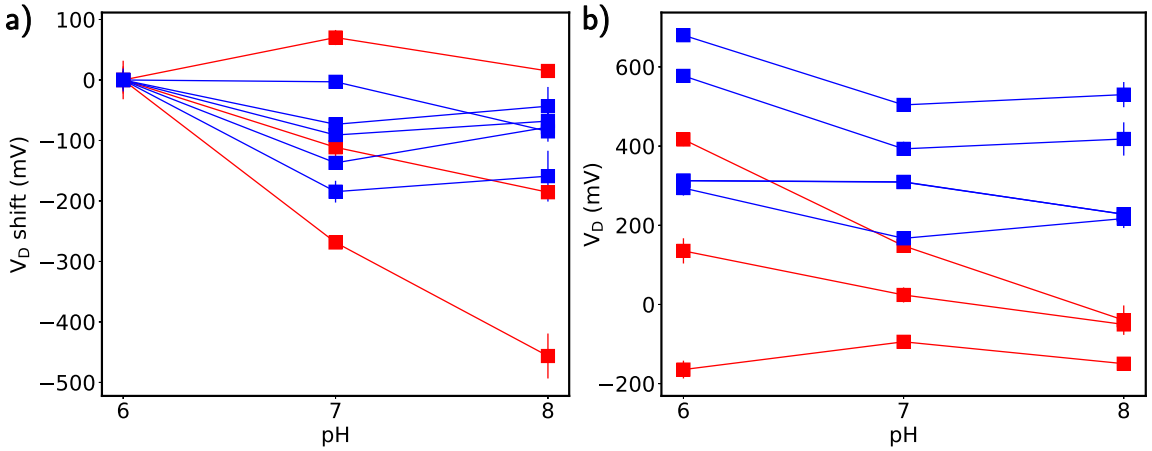

Fig. 2.23: All R(V_g) measurements for graphene/SiO_2 samples. Red are the samples without additional annealing and blue are samples after additional annealing. a) Dirac point shifts relative to pH 6. b) Absolute values of Dirac points. The error bar caps were excluded from the figures for better clarity.

parylene samples. The ΔV_D is (-99 ± 88) mV from pH 6 to pH 7; (-133 ± 123) mV from pH 6 to pH 8 and overall change is (67 ± 55) mV/pH. However, we should carefully evaluate these results. The sensitivity seems higher than for graphene/parylene samples, but the error for the measured values is nearly as high as the values themselves. Another point is that there are eight measurements and two of them have extreme values ($\sim$ 93 mV/pH and $\sim$ 228 mV/pH). Especially the second value is remarkably high. We wanted to study these samples further in $R(t)$ measurement but the sample devaluated through the measurements and lost the electrical contact. Thus, we could not even repeat $R(V_g)$ measurement to observe if such sensitivity is reproducible.

Back gate voltage $R(V_g)$ measurement

Graphene/SiO_2 sample construction (Figs. 2.2, 2.17) allows to use back gate voltage for characterizing the sample. Initially, we were careful in doing this experiment as the back gate was the first possible explanation of the sample devaluation. We stopped using the back gate in the beginning, until we found out the problem with water droplet cracking graphene. The back gating attempts were repeated after thermal annealing of four samples.

This set of samples was more durable and was not destroyed immediately. We did

several back gate measurements, but we did not detect the Dirac point. The samples were measured after more than 24 hours since annealing. In Fig. 2.24b are shown both back and top gate measurements. This measurement (blue) was done on a dry sample without the solution. We wanted to prevent possible damage of graphene by having high electric field near the buffer solution. The field effect is visible by resistance increase with increasing gate voltage. However, we had not reached the Dirac point and did not want to use higher gate voltages to prevent a destruction of SiO_2 layer.
The sample's Dirac point was found by top liquid gate (294 ± 11) mV that means heavy p-doping of the sample. Moreover, all annealed samples were heavily p-doped with $V_{\mathrm{D}} > 300\,\mathrm{mV}$, Tab. 2.3. Such p-doping is in agreement with discovery of Ni et al. [87], see Fig. 2.24a.
They did thermal annealing at temperature 500 °C in vacuum 0.5 Pa. The sample was cooled down in the chamber and exposed to air ambient. A considerable number of H_2O and O_2 molecules adsorbed on the surface and heavily doped graphene. H_2O and O_2 are electron acceptors, thus, p-doping graphene. Reversed doping can be achieved with the atmosphere of NH_3, NO_2 or CO and the doping level can be controlled by the annealing temperature, reported in [87]. Such a method allows us to control graphene doping.
We were not able to localise back gate Dirac point for the dry sample. Therefore, we wanted to use the advantage of electrochemical doping by pH buffers. Based on previous results, the higher pH shifts V_D towards negative values. We applied pH 7 on the sample and measured the $R(V_{\mathrm{g}})$ using the back gate. We did not observe any change and the data were still very similar to Fig. 2.24b. Unfortunately, the sample got destroyed; most likely by voltage 100 V and pH buffer presence. We willingly used such an extreme voltage because this sample had the lowest p-doping, Tab. 2.3. Thus, it was the best candidate for finding back gate V_{D}. It could have been interesting to use the back gate to divide electrochemical (pH buffers) and electrical (field effect) doping. The liquid top gate has both types at one place and it could have been interesting to compare it.

Tab. 2.3: Graphene/SiO_2 samples after annealing. Values are for pH 6 buffer.

sample (date)	$\mathbf{V_D}$ **(mV)**
11 (18.6.)	406 ± 15
11 (20.6.)	313 ± 1
12 (20.6.)	294 ± 11
13 (20.6.)	577 ± 13
14 (20.6.)	680 ± 13

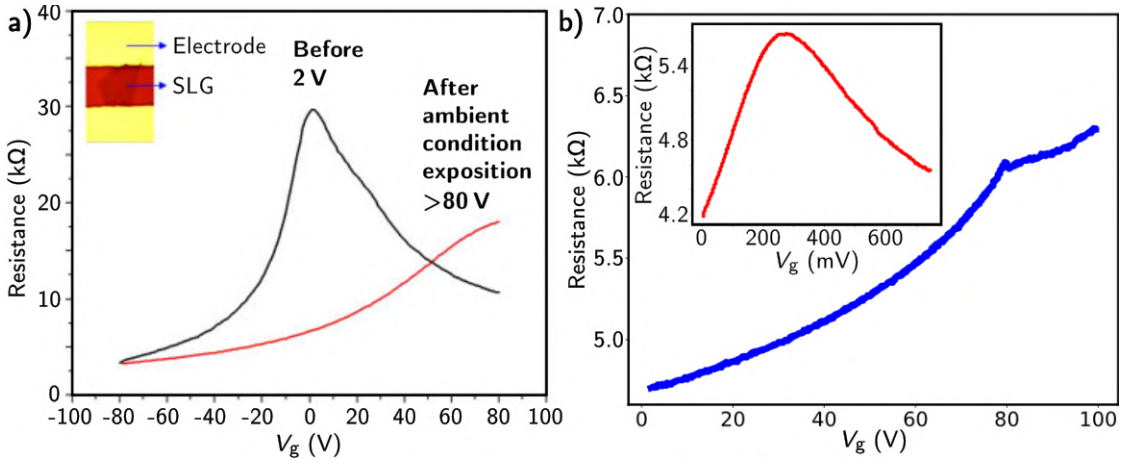

Fig. 2.24: Back gate graphene/SiO_2 results. a) Figure from reference studying effect of thermal annealing [87]. b) Our $R(V_g)$ measurement on one sample. Both curves are after annealing. Blue is result for back gate. Inset is top liquid gate $R(V_g)$ curve

$R(t)$ experiment

The resistance change is the main phenomena happening during the graphene/SiO_2 degradation. We are also doing more changes of the solution and DI water stirrings, thus, it is more invasive to the graphene layer. As we described in the challenges, we observed samples malfunction mostly during $R(t)$ measurements and our data are limited for $R(t)$ experiment. Due to the frequent sample destruction, we do not have sufficient data for statistical processing. We were successful with measurement of one thermally annealed sample, see Fig. 2.25. It is compelling that the difference between pH solutions is a few percent of resistance for DI water (R_0). It is much lower when compared to graphene/parylene tens of percent. The resistance is the highest for the lowest pH, same as for the graphene/parylene samples.

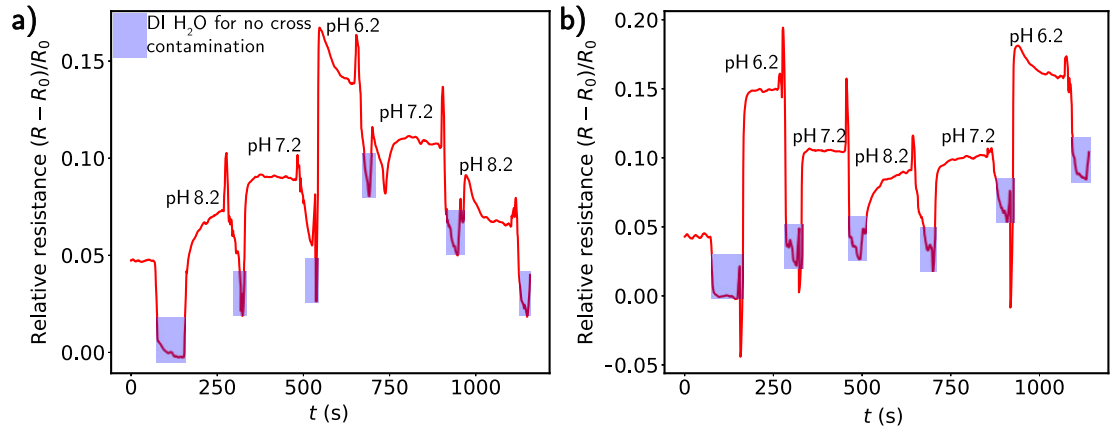

Fig. 2.25: $R(t)$ measurement of the thermally annealed graphene/SiO_2 sample.

2.5.3 Results summary

The only results suitable for valid comparison are $R(V_g)$ experiments where we did sufficient number of measurements, Fig. 2.26a. Final sensitivity is (23 ± 9) mV/pH for graphene/parylene samples and (67 ± 55) mV/pH for graphene/SiO_2 samples. The samples notably varied in the sensitivity and realizing more measurements could help us to obtain more data and lower measurement error. Especially, the result for graphene/SiO_2 should be interpreted carefully. Clearly visible in Fig. 2.26a is V_D shift to negative values with increasing pH.

The theory of electrochemical doping can be understood in Fig. 2.27. In acidic

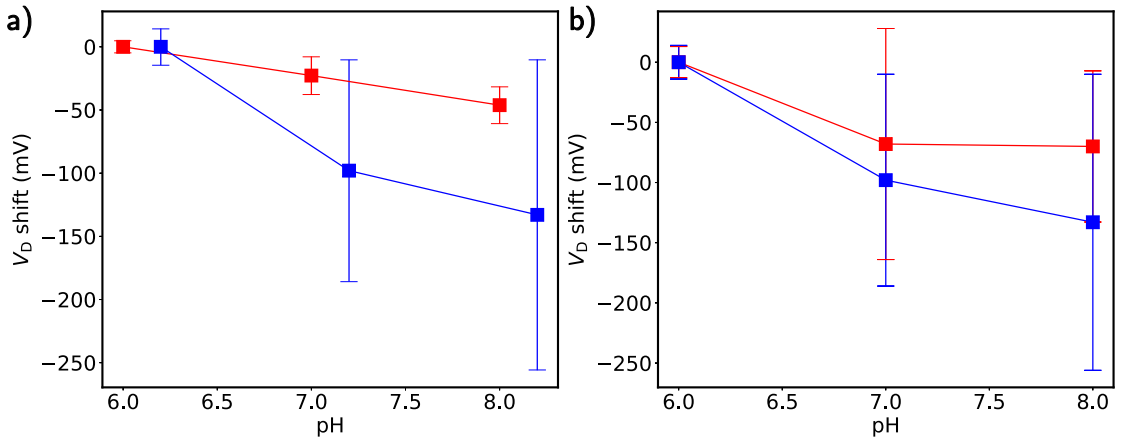

Fig. 2.26: a) $R(V_g)$ measurements summary for both type of samples. Red is graphene/parylene, blue is graphene/SiO_2. b) Comparison of graphene/SiO_2 sample results with (blue) and without (red) outliers.

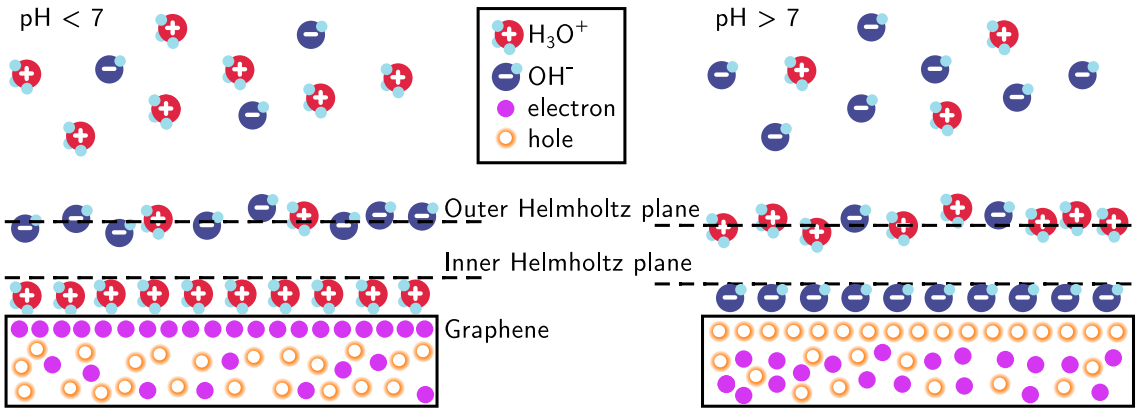

Fig. 2.27: Electrochemical doping by EDL. Left: Electron (n) doping in acidic solution (more H_3O^+) ions. Right: Hole (p) doping in alcaline solution (more OH^-).

solutions (pH < 7) is more H_3O^+ than OH^- ions. The ions adsorbtion process is capacitive and forms the EDL at the graphene surface. Ion layer at inner Helmholtz plane affects electrons in graphene layer. When there is more H_3O^+ ions (acidic solution) at inner Helmholtz plane, the graphene is n-doped and p-doped for OH^- ions

(alcaline solution) [64]. Fig. 2.27 describes processes happening at the graphene/solution interface. Next Fig. 2.28 transfers this knowledge further to $R(V_g)$ experiment.

The initial state is p-doped graphene with Fermi energy E_F lower than Dirac point V_D. First, we applied the pH 6 buffer and measured $R(V_g)$ curve. After that, we cleaned the sample with DI water and applied pH 8 buffer. The pH 8 buffer has a higher concentration of hydroxide OH^- ions. Based on the theory introduced in Fig. 2.27, more OH^- ions p-dope graphene and shift $R(V_g)$ curve to positive voltage and shift E_F deeper to valence band (red curve and image). This shift for increasing pH is reported in [64][88][65].

Our $R(t)$ data are also in an agreement with the results from $R(t)$ measurements.

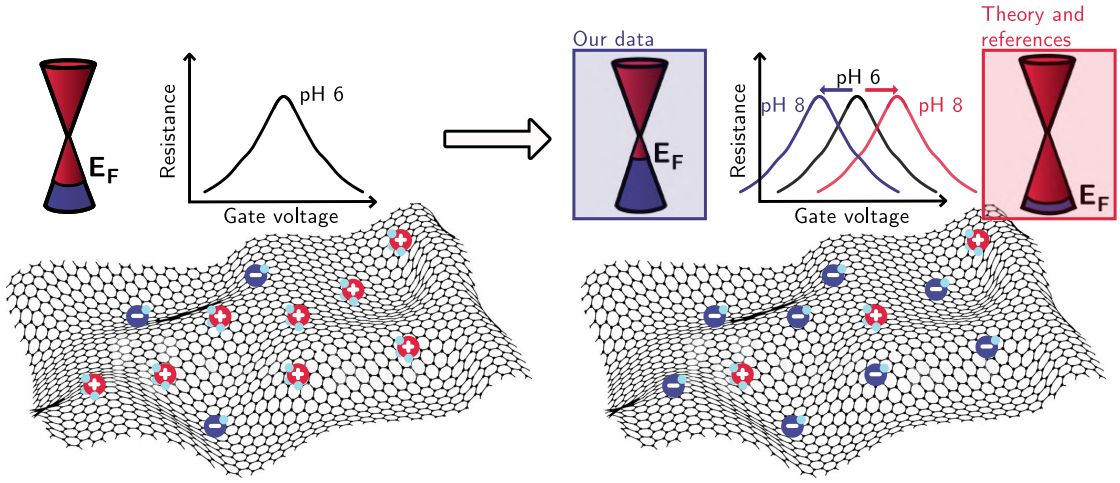

Fig. 2.28: Theory of $R(V_g)$ curve movement. Left: Initial state of p-doped graphene. Right: $R(V_g)$ curve movement with increased pH. Blue are our data and red is for the theory and mentioned references. Background graphene image taken from [91].

For $R(t)$ measurements, the solution is gate free ($V_g \sim 0\,V$) and nearly all samples are p-doped. Therefore, when we increase pH, $R(V_g)$ curve shifts to positive values and resistance decreases (Fig. 2.25, Fig. 2.13 and others) because we are still at $V_g = 0\,V$.

Many different aspects are influencing the $R(V_g)$ measurement. Cited references are using exfoliated [64], CVD [88] and epitaxially grown [65] graphene transferred on SiO_2 substrate. We did more measurements with higher statistical strength for parylene C, which is a polymer and can affect the measurement. It would be ideal to create samples on two different substrates (parylene and SiO_2) from the same graphene sheet and compare them. This could show us the exact influence of the substrate on experiment results. We performed experiments on two different substrates but the graphene quality was always different. We carried out many measurements for graphene/parylene samples and its results are significant. The substrate can really be a factor causing the change in the opposite direction. For graphene/SiO_2 samples, we also report V_D shift in the opposite direction than explains the theory and other references. We should be careful with interpreting these

results because of the extremely high error. Two measurements showed extraordinary sensitivity and we compared the results with and without them, Fig. 2.26b. The red curve represents results without outliers and still shows considerable error. The sensitivity is $(67 \pm 53)\,\mathrm{mV/pH}$ with outliers and $(35 \pm 52)\,\mathrm{mV/pH}$ without outliers for 95 % confidence interval. The values are overlapping between each other and are also near value V_D shift = 0. Thus, it is possible that the V_D shift can be in the opposite direction.

EDL is the essential principle of the liquid top gate. Kwon et al. reported that surface hydrophilicity influences EDL layer thickness, thus, its capacitance. The EDL thickness is higher for hydrophobic materials. Parylene is hydrophobic polymer [89] and graphene's wettability transparency is securing that it is more hydrophobic than graphene on SiO_2. However, this is not explaining why is the direction of V_D shift opposite because EDL capacitance should influence only sensitivity [83]. It is still worth mentioning for an illustration how is the system complex.

Moreover, Minot et al. [90] report a strong influence of gating electrode on the measurement results. Different electrodes shifted V_D curve and even changed sensor resistivity. We used a tungsten electrode for experiments in Grenoble and gold-coated electrode in Brno. It would be enriching to make the measurement on one sample with various electrodes.

To sum it up, the graphene was sensitive to pH. Resistance decrease in $R(t)$ experiments is in agreement with the theory and other references. The $R(V_\mathrm{g})$ experiment exhibits opposite behaviour which can be caused by many different aspects mentioned above. We recommend to perform individual experiments for each aspect and mainly focus on studying parylene and SiO_2 substrate covered with the same graphene sheet.

Conclusion

This thesis aimed to fabricate and characterise pH sensor based on graphene. We chose graphene on polymer parylene C as one of the substrates because it is a flexible and biocompatible material. It is a proper choice in terms of the future application, a wound condition monitoring patch. We also used graphene on SiO_2 for comparison with graphene on parylene C. Graphene is a sensitive material which can be easily doped. We used the liquid top gate to characterise sample doping level and the position of Dirac point as a function of pH. The second experiment measured resistance change caused by different pH as a function of time.
The results confirmed graphene sensitivity to various pH. The Dirac point shifted towards negative values with increasing pH. At the same time, increasing pH was decreasing the sample resistance. Additional functionalisation with polyaniline (PANI) was also successful, and it was sensitive to pH. However, we were not able to characterise the functionalised sample by gate field effect. The main obstacle was probably the thickness of the PANI coating. We wanted to functionalise graphene/SiO_2 because we assumed spin-coated PANI on SiO_2 may have lower thickness. This goal had to be cancelled due to coronavirus lock-down complications.
The thesis covers many topics and offers various proposals for additional research. Based on the results, the graphene/parylene C samples were durable and repeatedly measured. It was not true for graphene/SiO_2 samples which got damaged by water. Significant attention should be focused on the fabrication process and graphene adhesion on SiO_2. It is very limiting when the samples are destroyed during measurement and we can not repeat measurements. Thus, we verified that thermal annealing in the vacuum prevents graphene destruction by water. Sensitivity was considerably different for each sample and it would be ideal to measure many samples with the same graphene quality. However, persistent production of graphene of the same quality is still a challenge in the graphene community. There is a significant progress in the CVD graphene fabrication but resistivity, grain sizes, number of residues and impurities is always a little bit different.
Study of ionic strength also deserves considerable attention. The ionic strength is changing EDL thickness. Thus, it can affect OH^- and H_3O^+ mirroring effect as the EDL thickness is decreased with higher ionic strength. Therefore, the pH sensor can be more sensitive to higher ionic strength or contrary.
It was revealed that graphene is sensible to various pH. However, we should be careful with interpreting this sensitivity because graphene is a two-dimensional (2D) material created only by its surface. Therefore, it is simple to change its properties by all adsorbates. Graphene sensitivity and simple functionalisation can be used to our advantage. Graphene can serve as a sensitive layer and proper agents can make graphene sensitive only to a specific analyte as referred in [92][93][94]. Therefore, we verified successful functionalisation with PANI but further study was out of the scope of this thesis.
For future studies, we propose to study graphene functionalisation deeply. The graphene sensitivity is verified in many studies, but it is the functionalisation that can make it useful in applications. Graphene is a novel material with several possible applications but there are still many challenges that have to be resolved.

Bibliography

[1] FRYKBERG, Robert G.; BANKS, Jaminelli. Challenges in the treatment of chronic wounds. Advances in wound care, 2015, 4.9: 560-582.

[2] FRADEN, Jacob. Handbook of modern sensors: physics, designs, and applications. 5th ed. New York: Springer, 2016. ISBN 9781441964663.

[3] DRAVIS, C. Ephs, Ephrins, and Bidirectional Signaling. Nature Education, 2010, 3(9):22

[4] YOON, Jeong-Yeol. Introduction to biosensors: from electric circuits to immunosensors. New York: Springer, c2013. ISBN 978-1-4419-6021-4.

[5] MCEWEN, Adrian a Hakim CASSIMALY. Designing the Internet of Things. 1. Chichester: John Wiley, 2014. ISBN 978-1-118-43062-0.

[6] SKLÁDAL, Petr. Biosensory, Masarykova univerzita, Brno 2002 (CS)

[7] Microcontroller Unit Shipments Surge but Falling Prices Sap Sales Growth. In: IC Insights [online]. Scottsdale, Arizona UDS: IC Insights, 2015 [cit. 2020-02-29]. Available from: https://www.icinsights.com/news/bulletins/Microcontroller-Unit-Shipments-Surge-But-Falling-Prices-Sap-Sales-Growth/

[8] TURNER, A. P. F. Biosensors: sense and sensibility. Chemical Society Reviews, 2013, 42(8), 3184.

[9] MEHROTRA, P. (2016). Biosensors and their applications - A review. Journal of Oral Biology and Craniofacial Research, 6(2), 153–159.

[10] UNNIKRISHNAN, B., PALANISAMY, S., CHEN, S. M. A simple electrochemical approach to fabricate a glucose biosensor based on graphene-glucose oxidase biocomposite. Biosensors and Bioelectronics, 2013, 39(1), 70–75.

[11] WANG, L., GAO, X., JIN, L., WU, Q., CHEN, Z., LIN, X. Amperometric glucose biosensor based on silver nanowires and glucose oxidase. Sensors and Actuators, B: Chemical, 2013, 176, 9–14.

[12] LI, H., HE, J., ZHAO, Y., WU, D., CAI, Y., WEI, Q., YANG, M. Immobilization of glucose oxidase and platinum on mesoporous silica nanoparticles for the fabrication of glucose biosensor. Electrochimica Acta, 2011, 56(7), 2960–2965.

[13] KARYAKIN, A. A., GITELMACHER, O. V., KARYAKINA, E. E. Prussian Blue-Based First-Generation Biosensor. A Sensitive Amperometric Electrode for Glucose. Analytical Chemistry, 1995, 67(14), 2419–2423.

[14] GARJONYTE, R., MALINAUSKAS, A. Amperometric glucose biosensors based on Prussian Blue- and polyaniline-glucose oxidase modified electrodes. Biosensors and Bioelectronics, 2000, 15(9–10), 445–451.

[15] JACOBS, M., MUTHUKUMAR, S., PANNEER SELVAN, A., ENGEL CRAVEN, J., PRASAD, S. Ultra-sensitive electrical immunoassay biosensors using nanotextured zinc oxide thin films on printed circuit board platforms. Biosensors and Bioelectronics, 2014, 55, 7–13.

[16] AHN, K. C., KIM, H. J., MCCOY, M. R., GEE, S. J., HAMMOCK, B. D. Immunoassays and biosensors for monitoring environmental and human exposure to pyrethroid insecticides. Journal of Agricultural and Food Chemistry, 2011, 59(7), 2792–2802.

[17] WANG, K., SUN, Z., FENG, M., LIU, A., YANG, S., CHEN, Y., LIN, X. Design of a sandwich-mode amperometric biosensor for detection of PML/RAR fusion gene using locked nucleic acids on gold electrode. Biosensors and Bioelectronics, 2011, 26(6), 2870–2876.

[18] BRIONES, C., MORENO, M. Applications of peptide nucleic acids (PNAs) and locked nucleic acids (LNAs) in biosensor development. Analytical and Bioanalytical Chemistry, 2012, 402(10), 3071–3089.

[19] LIU, A., WANG, K., WENG, S., LEI, Y., LIN, L., CHEN, W., LIN, X., CHEN, Y. Development of electrochemical DNA biosensors. TrAC - Trends in Analytical Chemistry, 2012, 37, 101–111.

[20] GRIESHABER, D., MACKENZIE, R., VÖRÖs, J., REIMHULT, E. Electrochemical Biosensors - Sensor Principles and Architectures. Sensors, 2008, 8, 1400-1458.

[21] TURNER, A. "Biosensors: Then and Now." Trends in Biotechnology, 2013, vol.31, no. 3.

[22] MADRID, R. E., CHEHÍN, R., CHEN, T.-H., GUISEPPI-ELIE, A. Biosensors and Nanobiosensors. 2017, 391–462.

[23] KROTO, H. W., HEATH, J. R., O'BRIEN, S. C., CURL, R. F., SMALLEY, R. E. C60: Buckminsterfullerene. Nature, 1985, 318(6042), 162–163.

[24] KROTO, H. W. The stability of the fullerenes Cn, with n= 24, 28, 32, 36, 50, 60 and 70. Nature, 1987, 329.6139: 529-531.

[25] PISKOTI, C.; YARGER, Jeffery; ZETTL, A. C 36, a new carbon solid. Nature, 1998, 393.6687: 771-774.

[26] ALA'A, K., et al. Isolation, separation and characterisation of the fullerenes C 60 and C 70: the third form of carbon. Journal of the Chemical Society, Chemical Communications, 1990, 20: 1423-1425.

[27] MADOU, Marc J. Fundamentals of Microfabrication and Nanotechnology, Three-Volume Set. CRC Press, 2018.

[28] DRESSELHAUS, Mildred S.; DRESSELHAUS, Gene; EKLUND, Peter C. Science of fullerenes and carbon nanotubes: their properties and applications. Elsevier, 1996.

[29] NETO, Antonio Castro; GUINEA, Francisco; PERES, Nuno Miguel. Drawing conclusions from graphene. Physics World, 2006, 19.11: 33.

[30] AMBROSI, Adriano, et al. Graphene and its electrochemistry–an update. Chemical Society Reviews, 2016, 45.9: 2458-2493.

[31] NETO, AH Castro, et al. The electronic properties of graphene. Reviews of modern physics, 2009, 81.1: 109.

[32] NOVOSELOV, Kostya S., et al. Electric field effect in atomically thin carbon films. science, 2004, 306.5696: 666-669.

[33] BALANDIN, Alexander A., et al. Superior thermal conductivity of single-layer graphene. Nano letters, 2008, 8.3: 902-907.

[34] BUNCH, J. Scott, et al. Impermeable atomic membranes from graphene sheets. Nano letters, 2008, 8.8: 2458-2462.

[35] NAIR, Rahul Raveendran, et al. Fine structure constant defines visual transparency of graphene. Science, 2008, 320.5881: 1308-1308.

[36] LEE, C., WEI, X., KYSAR, J. W., HONE, J. Measurement of the elastic properties and intrinsic strength of monolayer graphene. Science, 2008 321(5887), 385–388.

[37] ZHANG, Peng, et al. Fracture toughness of graphene. Nature communications, 2014, 5: 3782.

[38] JUNG, GangSeob; QIN, Zhao; BUEHLER, Markus J. Molecular mechanics of polycrystalline graphene with enhanced fracture toughness. Extreme Mechanics Letters, 2015, 2: 52-59.

[39] PAPAGEORGIOU, D. G., KINLOCH, I. A., YOUNG, R. J. Mechanical properties of graphene and graphene-based nanocomposites. Progress in Materials Science, 2017, 90, 75–127.

[40] ANDO, Tsuneya. The electronic properties of graphene and carbon nanotubes. NPG asia materials, 2009, 1.1: 17-21.

[41] ANDO, Tsuneya. Screening effect and impurity scattering in monolayer graphene. Journal of the Physical Society of Japan, 2006, 75.7: 074716-074716.

[42] KIREEV, Dmitry. Combining graphene and organic ferroelectric for possible memory devices. Thesis for the Degree of Erasmus Mundus Master of Nanoscience and Nanotechnology Chalmers University of Technology KULeuven, 2013.

[43] MARTIN, Jens, et al. Observation of electron–hole puddles in graphene using a scanning single-electron transistor. Nature physics, 2008, 4.2: 144-148.

[44] WOLF, Edward L. Graphene: a new paradigm in condensed matter and device physics. OUP Oxford, 2013.

[45] LI, Xuesong, et al. Large-area synthesis of high-quality and uniform graphene films on copper foils. science, 2009, 324.5932: 1312-1314.

[46] CHANG, Y. M., KIM, H., LEE, J. H., SONG, Y.-W. Multilayered graphene efficiently formed by mechanical exfoliation for nonlinear saturable absorbers in fiber mode-locked lasers. Applied Physics Letters, 2010, 97(21), 211102.

[47] YOSHIHARA, Naoki; NODA, Masaru. Chemical etching of copper foils for single-layer graphene growth by chemical vapor deposition. Chemical Physics Letters, 2017, 685: 40-46.

[48] FEILI, Dara, et al. Flexible organic field effect transistors for biomedical microimplants using polyimide and parylene C as substrate and insulator layers. Journal of micromechanics and microengineering, 2006, 16.8: 1555.

[49] STIEGLITZ, T., et al. Encapsulation of flexible biomedical microimplants with parylene C. In: IFESS. 2002. p. 2002.

[50] STARK, Nancy. Literature review: biological safety of parylene C. Medical Plastic and Biomaterials, 1996, 3: 30-35.

[51] HINOJOZA, Jake. Parylene: The Types and Uses. Advanced Coating [online]. California, 2017 [cit. 2020-06-04]. Available from: https://www.advancedcoating.com/blog/parylene-the-types-and-uses

[52] LAIRD, Joyce. Parylene Coating Helps Extend Life Of Medical Sensors. In: Medical Design Outsourcing [online]. 2018 [cit. 2020-06-04]. Dostupné z: https://www.medicaldesignandoutsourcing.com/parylene-coating-helps-extend-life-of-medical-sensors/

[53] PARYLENE THICKNESS – WHEN A LITTLE GOES A LONG WAY. Vsi-Parylene [online]. Broomfield, Colorado 80021: VsiParylene, 2018 [cit. 2020-06-03]. Available from: https://vsiparylene.com/2018/04/15/parylene-thickness/

[54] VON HELMHOLTZ, H. L. F. Studies of electric boundary layers. Wied. Ann, 1879, 7: 337-382.

[55] RIEGER, P. H. Electrochemistry (2nd ed.). Chapman Hall, 1994.

[56] BROWN, M. A., Goel, A., Abbas, Z. Effect of Electrolyte Concentration on the Stern Layer Thickness at a Charged Interface. Angewandte Chemie - International Edition, 2016, 55(11), 3790–3794.

[57] MILLER, J. R., SIMON, P. Materials science: Electrochemical capacitors for energy management. Science, 2008, 321(5889), 651–652.

[58] TAKAHARA, E., WAKASA, T., YAMADA, J. A study for electric double layer capacitor (EDLC) application to railway traction energy saving including change over between series and parallel modes. Proceedings of the Power Conversion Conference-Osaka 2002, PCC-Osaka 2002, 2, 855–860.

[59] ZEGUINE, C., RANAWEERA, C. K., WANG, Z., DVORNIC, P. R., KAHOL, P. K., SINGH, S., TRIPATHI, P., SRIVASTAVA, O. N., SINGH, S., GUPTA, B. K., GUPTA, G., GUPTA, R. K. High-Performance Flexible Supercapacitors obtained via Recycled Jute: Bio-Waste to Energy Storage Approach. Scientific Reports, 2017, 7(1), 1–12.

[60] CHOI, N. S., CHEN, Z., FREUNBERGER, S. A., JI, X., SUN, Y. K., AMINE, K., YUSHIN, G., NAZAR, L. F., CHO, J., BRUCE, P. G. Challenges facing lithium batteries and electrical double-layer capacitors. Angewandte Chemie - International Edition, 2012, 51(40), 9994–10024.

[61] HAMMOND, Jules L.. "Micro- and nanogap based biosensors.", 2017.

[62] GIERA, B., HENSON, N., KOBER, E. M., SHELL, M. S., SQUIRES, T. M. Electric double-layer structure in primitive model electrolytes: Comparing molecular dynamics with local-density approximations. Langmuir, 2015, 31(11), 3553–3562.

[63] JIANG, G., CHENG, C., LI, D., LIU, J. Z. Molecular dynamics simulations of the electric double layer capacitance of graphene electrodes in mono-valent aqueous electrolytes. Nano Research, 2016, 9(1), 174–186.

[64] LEI, Nan, et al. Simple graphene chemiresistors as pH sensors: fabrication and characterization. Measurement science and technology, 2011, 22.10: 107002.

[65] ANG, Priscilla Kailian, et al. Solution-gated epitaxial graphene as pH sensor. Journal of the American Chemical Society, 2008, 130.44: 14392-14393.

[66] HELLER, Iddo, et al. Influence of electrolyte composition on liquid-gated carbon nanotube and graphene transistors. Journal of the American Chemical Society, 2010, 132.48: 17149-17156.

[67] WANG, Xiaodan, et al. CVD graphene as an electrochemical sensing platform for simultaneous detection of biomolecules. Scientific reports, 2017, 7.1: 1-9.

[68] CHIA, Joanna Su Yuin, et al. A bio-electrochemical sensing platform for glucose based on irreversible, non-covalent pi–pi functionalization of graphene produced via a novel, green synthesis method. Sensors and Actuators B: Chemical, 2015, 210: 558-565.

[69] ZHANG, Chunmei, et al. Graphene-based Electrochemical Glucose Sensors: Fabrication and Sensing Properties. Electroanalysis, 2018, 30.11: 2504-2524.

[70] LEE, Hyunjae, et al. A graphene-based electrochemical device with thermoresponsive microneedles for diabetes monitoring and therapy. Nature nanotechnology, 2016, 11.6: 566.

[71] WEI, Shijing, et al. Transfer-free CVD graphene for highly sensitive glucose sensors. Journal of Materials Science Technology, 2020, 37: 71-76.

[72] ONO, Sayaka, et al. Increased wound pH as an indicator of local wound infection in second degree burns. Burns, 2015, 41.4: 820-824.

[73] GETHIN, Georgina, et al. The significance of surface pH in chronic wounds. Wounds uk, 2007, 3.3: 52.

[74] LIU, Yingjun, et al. Rapid roll-to-roll production of graphene film using intensive Joule heating. Carbon, 2019, 155: 462-468.

[75] AMIRI, Ahmad, et al. Facile, environmentally friendly, cost effective and scalable production of few-layered graphene. Chemical Engineering Journal, 2017, 326: 1105-1115.

[76] CyberScan pH 1500. In: Thermo Fisher Scientific Inc. [online]. [cit. 2020-06-17]. Available from: https://www.eutechinst.com/images/CyberScanpH1500.jpg

[77] SHINWARI, Waleed et al. Microfabricated Reference Electrodes and Their Biosensing Applications. Sensors (Basel, Switzerland), 2017, 1679-715. 10.3390/s100301679.

[78] SHIPMAN JR, Charles. Evaluation of 4-(2-hydroxyethyl)-1-piperazineëthanesulfonic acid (HEPES) as a tissue culture buffer. Proceedings of the Society for experimental biology and medicine, 1969, 130.1: 305-310.

[79] SKOOG, Douglas A., et al. Fundamentals of analytical chemistry. Nelson Education, 2013.

[80] Acid-Base Titration Curves. Chemistry LibreTexts [online]. University of California: UC Davis Library, 2019 [cit. 2020-04-28]. Available from: https://chem.libretexts.org/

[81] RAHIMI, Rahim, et al. A low-cost flexible pH sensor array for wound assessment. Sensors and Actuators B: Chemical, 2016, 229: 609-617.

[82] RAFIEE, Javad, et al. Wetting transparency of graphene. Nature materials, 2012, 11.3: 217-222.

[83] KWON, Sun Sang, et al. Electrical Double Layer of Supported Atomically Thin Materials. Nano letters, 2019, 19.7: 4588-4593.

[84] HONG, Guo, et al. On the mechanism of hydrophilicity of graphene. Nano letters, 2016, 16.7: 4447-4453.

[85] HAN, Zheng. Macroscopic CVD graphene for nanoelectronic: from growth to proximity induced 2D superconductivity. 2013. PhD Thesis. Doctoral dissertation, CNRS.

[86] CHEN, Jian-Hao, et al. Defect scattering in graphene. Physical review letters, 2009, 102.23: 236805.

[87] NI, Zhen Hua, et al. The effect of vacuum annealing on graphene. Journal of Raman Spectroscopy: An International Journal for Original Work in all Aspects of Raman Spectroscopy, Including Higher Order Processes, and also Brillouin and Rayleigh Scattering, 2010, 41.5: 479-483.

[88] MAILLY-GIACCHETTI, Benjamin, et al. pH sensing properties of graphene solution-gated field-effect transistors. Journal of Applied Physics, 2013, 114.8: 084505.

[89] WEI, Lai, et al. Thickness-controlled hydrophobicity of fibrous Parylene-C films. Materials Letters, 2010, 64.9: 1063-1065.

[90] MINOT, Ethan D., et al. Carbon nanotube biosensors: The critical role of the reference electrode. Applied Physics Letters, 2007, 91.9: 093507.

[91] Graphene, a molecular network of hexagons connected together. In: Adobe Stock [online]. [cit. 2020-06-22]. Available from: https://stock.adobe.com/cz/

[92] LUAN, Feng, et al. CoS2-decorated ionic liquid-functionalized graphene as a novel hydrazine electrochemical sensor. Talanta, 2018, 182: 529-535.

[93] YANG, Jianping, et al. A novel nonenzymatic glucose sensor based on functionalized PDDA-graphene/CuO nanocomposites. Sensors and Actuators B: Chemical, 2017, 253: 1087-1095.

[94] TSANG, Deana Kwong Hong, et al. Chemically functionalised graphene FET biosensor for the label-free sensing of exosomes. Scientific reports, 2019, 9.1: 1-10.

List of abbreviations

PC	Portable Computer
RAM	Random Access Memory
IoT	Internet of Things
LOD	Limit of Detection
GOx	Glucose oxidase
DNA	Deoxyribonucleic acid
RNA	Ribonucleic acid
CNT	Carbon nanotube
AFM	Atomic Force Microscopy
FIB	Focused Ion Beam
CVD	Chemical vapour deposition
PMMA	Poly(methyl methacrylate)
CVDP	Chemical vapour deposition polymerization
EDL	Electric Double Layer
EDLCs	Electric double layer capacitors
SWNTs	Single-walled carbon nanotubes
DPV	Differential pulse voltammetry
AA	Ascorbic acid
DA	Dopamine
UA	Uric acid
Trp	Tryptophan
DI	Deionized
CEITEC	CentralEuropean Institute of Technology
CNRS	Le Centre national de la recherche Scientifique
IPE	Institute of Physical Engineering
BUT	Brno University of Technology
PANI	Polyaniline

ES	Emeraldine salt
EB	Emeraldine base